LARGE ANGLE SCATTERING OF H^+ AND H_2^+ BY ARGON

by

Everrette Verne Snotherly

United States
Naval Postgraduate School

THESIS

LARGE ANGLE SCATTERING OF H^+ AND H_2^+

BY ARGON

by

Everrette Verne Snotherly, Jr.

October 1969

Large Angle Scattering of H^+ and H_2^+ by Argon

by

Everrette Verne Snotherly, Jr.
Lieutenant, United States Navy
B.A., Duke University, 1961

Submitted in partial fulfillment of the
requirements for the degree of

MASTER OF SCIENCE IN PHYSICS

from the

NAVAL POSTGRADUATE SCHOOL
October 1969

ABSTRACT

The elastic differential scattering cross sections for $\underline{H}^+$, $\underline{H}_2^+$ + Ar → $\underline{H}^+$, $\underline{H}_2^+$ + Ar were measured for angles of 39° to 50° with incident lab energy of 100 eV. The apparatus utilized the properties of axially symmetric, non-uniform magnetic fields (large thin solenoid) to focus all scattered ions with vector momentum $\vec{p}$ within $\Delta\vec{p}$ onto a detector placed down the magnetic axis. Thus, the solid angle was increased by a factor of about 300 over conventional methods with comparable resolution in $\Delta\theta$ (about 1°). A typical value for $\sigma_{H^+}(43^\circ)$ is 8.2×10^{-18} cm^2. The H^+ data was compared with data of Magnuson, et.al., via a scaling law and was in excellent agreement. A typical value for $\sigma_{H_2^+}(43^\circ)$ is 2.4×10^{-20} cm^2. A simple refinement of a classical model for H_2^+ scattering by Feist relates these cross sections by $\sigma_{H_2^+}(\theta) = P\,\sigma_{H^+}(\theta) \simeq \frac{4D}{\pi \ell^2 E_o} [\sigma_{H^+}(\theta)]^2$ where P is an orientation factor, D the binding energy, and ℓ the internuclear separation. This expression relates the cross sections to within the accuracy of the experiment thus verifying the classical approximations.

TABLE OF CONTENTS

I. INTRODUCTION---------- 9

II. THEORY----------11

A. THE MODEL----------11

B. CALCULATION OF $\sigma_{H^+}(\theta)$----------16

C. CALCULATION OF THE ORIENTATION PROBABILITY---------16

D. COMPUTER CALCULATION OF $\sigma_{H^+}(\theta)$ AND $\sigma_{H_2^+}(\theta)$----------21

III. EXPERIMENTAL APPARATUS----------23

A. GENERAL DESCRIPTION----------23

B. THE DUOPLASMATRON ION SOURCE----------25

C. THE MASS SPECTROMETER----------28

D. THE SCATTERING CELL----------30

E. THE FOCUSING MAGNET----------32

F. THE DETECTOR----------40

IV. EXPERIMENTAL RESULTS----------46

A. LABORATORY CROSS SECTION MEASUREMENT----------46

B. MEASUREMENT OF THE $\underline{H}^+ + Ar \rightarrow \underline{H}^+ + Ar$ CROSS SECTION--47

C. MEASUREMENT OF THE $\underline{H_2}^+ + Ar \rightarrow \underline{H_2}^+ + Ar$ CROSS SECTION-52

D. EXPERIMENTAL RESULTS AND THE CLASSICAL MODEL-------55

V. CONCLUSIONS----------59

APPENDIX A 1. Computer Program for $\sigma_{H^+}(\theta)$ and $\sigma_{H_2^+}(\theta)$-------62

2. Calculation for Ion Trajectory and Solid Angle----------68

LIST OF REFERENCES----------71

INITIAL DISTRIBUTION LIST----------72

FORM DD 1473----------73

LIST OF FIGURES

Figure

1. Protons With Same Impact Parameter but Different Scattering Planes----------13

2. Protons With the Same Scattering Plane but Different Impact Parameters----------15

3. a. Proton Velocity Difference Due to Difference in Impact Parameter----------19

b. Proton Velocity Difference Due to Difference in Scattering Plane----------19

4. Log of Scattering Cross Section vs Scattering Angle for $\underline{H}^+ + Ar \rightarrow \underline{H}^+ + Ar$ and $\underline{H}_2^+ + Ar \rightarrow \underline{H}_2^+ + Ar$----------22

5. Schematic of the Experimental Apparatus----------24

6. Duoplasmatron----------26

7. Circuit Diagram for Duoplasmatron----------27

8. Schematic of Mass Spectrometer----------29

9. The Scattering Cell and Beam Collector----------31

10. Magnetic Field Strength at Various Distances Along the Magnetic Axis for Various Currents----------34

11. Orbit of Charged Particle in Uniform Magnetic Field--35

12. Trajectories of H^+ ions, with 100 eV. Incident Energy Scattered by Argon, in Focusing Magnetic Field with I = 4.8 amps----------39

13. Detector Aperature Geometry----------41

14. The Bendix Model 306 Magnetic Electron Multiplier----42

15. Circuit Diagram for Electron Multiplier----------43

16. Multiplier Gain vs Magnetic Field----------45

17. Experimental Measurements of $\underline{H}^+ + Ar \rightarrow \underline{H}^+ + Ar$ at 100 eV----------48

18. Average of Experimental Measurements of $\underline{H}^+ + Ar \rightarrow \underline{H}^+ + Ar$ at 100 eV----------49

19. Experimental Measurements of $\underline{H}_2^+ + Ar \rightarrow \underline{H}_2^+ + Ar$ at 100 eV----------53

20. Average of Experimental Measurements of $\underline{H}_2^+ + Ar \rightarrow \underline{H}_2^+ + Ar$ at 100 eV----------54

21. Analysis of Experimental Measurement Assumming a Systematic Error----------57

22. Analysis of Experimental Measurement Assumming no Systematic Error----------58

ACKNOWLEDGEMENTS

I wish to express my most genuine gratitude to Dr. Otto Heinz, my advisor forthis experiment. Through his insight, reason was sifted out of chaos, and his enthusiasm for physics made this research project fun.

I am also indebted to Mr. Thomas Maris of the Physics Department technical staff who maintains the scattering apparatus, I am convinced that given a piece of metal and a sketch that Tom can build anything. He is a real craftsman.

I am grateful to Dr. G.D. Magnuson of the University of Virginia for relaying his data from a similar experiment. This greatly assisted in analyzing our own data.

I. INTRODUCTION

Atomic processes such as the scattering of complex ions by heavy atoms are properly described by quantum mechanics. Unfortunately, for a many-body problem the mathematics becomes untractable. In order to produce useful solutions approximations must be introduced. One class of approximations involves the use of semi-classical models of the collision process. By sacrificing rigor, useful solutions are obtained that still provide insight into the physical process involved.

The classical model investigated here is used to calculate the differential scattering cross section of the H_2^+ ion by a spherically symmetric potential. The theory was developed by Feist [1] based on the earlier work of Bates, Cook, and Smith [2] as follows. First, calculate the differential scattering cross section of a single proton from a spherically symmetric potential. Then calculate the probability that the second proton is oriented with respect to the first such that the H_2^+ molecule is not disrupted by the collision. The differential scattering cross section for H_2^+ is the product of this orientation probability times the cross section for the single proton.

The purpose of the experiment reported here was to test the theory as developed by Feist. This was done by measuring the differential scattering cross section of H^+ by Argon and

H_2^+ by Argon at incident energies of 100 eV and laboratory angles from 39^o to 49^o. Thus, the orientation probability was determined experimentally and compared with Feist's calculation.

II. THEORY

A. THE MODEL

This classical model is applicable to the scattering of the H_2^+ ion over a range of incident energies E_o (in laboratory coordinates) by a spherically symmetric potential such as heavy noble gas atoms. The reaction studied was $\underline{H_2^+} + Ar \rightarrow \underline{H_2^+} + Ar$ where the underline indicates the fast particle in laboratory coordinates. The two protons of the H_2^+ ion have an equilibrium separation in the ground state of 1.06 angstroms and a disassociation energy of 2.648 eV. The lower energy limit where this model could no longer be expected to apply would be where the incident ion energy becomes comparable with the ion binding energy. This requires that $E_o >> 2.648$ eV or $E_o \gtrsim 30$ eV. The upper energy limit where this model could no longer be expected to apply is governed by the uncertainty principle. In this application it is required that the de Broglie wavelength be much less than the distance of closest approach or $r_o >> \lambda_D = \frac{h}{mv_o}$ which may be written as $r_o \geq \frac{10h}{\sqrt{2mE_o}}$. Now r_o may be further related to E_o by considering a head-on collision with the shielded coulomb potential for Argon (this potential is discussed in Section II B, and Appendix A). Considering only the dominant term of the potential one can write

$$E_o = \frac{Ze^2}{r_o} Ae^{-\alpha r_o}$$

where A and α are parameters of the potential. Substituting

values for the constants one obtains

$$E_o = 14.6 \frac{1}{r_o^2}$$

$$\text{and} \quad E_o = 411 \frac{1}{r_o} e^{-1.68 r_o}$$

with E_o in units of eV and r_o in units of Bohr radii. The value of E_o that satisfies these equations is $E_o = 1.13 \times 10^4$ eV. This shows that a classical model for the scattering of H_2^+ should be valid for incident energies up to about 10 KeV.

In a scattering event the H_2^+ ion may be disrupted due to the following two effects. First, consider the two protons approaching a spherically symmetric potential with the same impact parameter, b. Using the concept of an impulse approximation, consider each proton-target collision separately, yielding a description in terms of two two-body collisions. Due to the spherical symmetry each proton scattered is confined to a plane defined by the scattering axis and a line from the scattering center to the proton. The angular difference between the scattering planes, $\Delta\emptyset$ will result in a difference in velocities of the two protons after scattering such that their relative energy may be greater than the binding energy and the H_2^+ ion will be disrupted. Figure 1 illustrates this process.

Second, consider the protons oriented such that they will be scattered in the same plane but with different impact parameters.

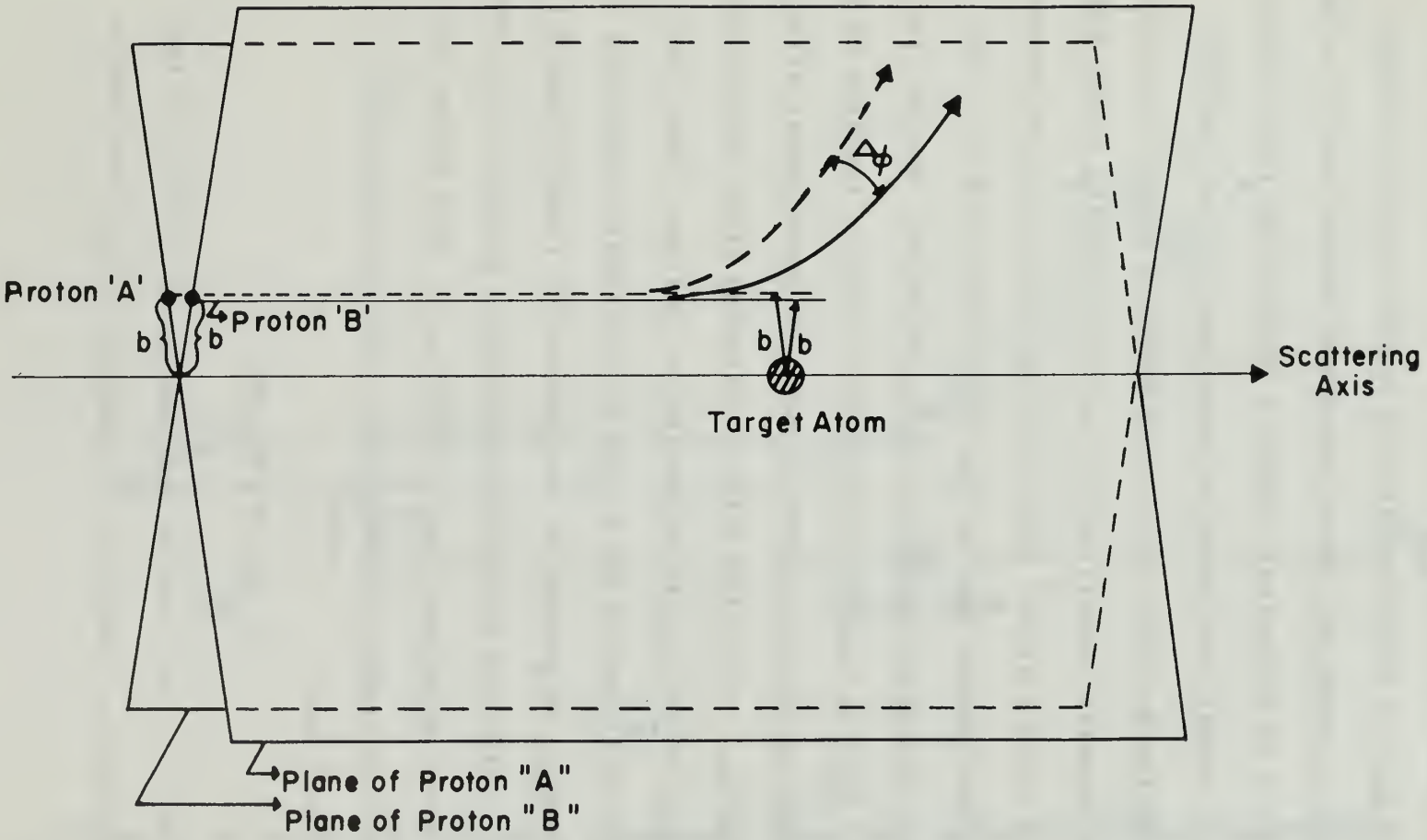

Figure 1. Protons with same impact parameter but different scattering planes.

This will result in a difference in scattering angle $\Delta\theta$ and therefore again a relative velocity between the two protons. The relative energy may again exceed the binding energy so that the ion will be disrupted. Figure 2 illustrates this process.

In the actual case these two processes are not separable and disruption may occur due to the combined effect of $\Delta\phi$ and $\Delta\theta$. The necessary condition for the ion remaining intact after collision is $D > \frac{1}{2}\mu(\Delta V)^2$ where D is the disassociation energy, $\mu = M_p/2$ the reduced mass of the two protons, and ΔV is the difference in velocities due to both $\Delta\phi$ and $\Delta\theta$. Whether the $\underline{H}_2^+ + Ar \rightarrow \underline{H}_2^+ + Ar$ reaction will occur is then a function of the orientation of the two protons before (or equivalently after) the collision. The differential scattering cross section for the H_2^+ ion, $\sigma_{H_2^+}(\theta)$ may be calculated as follows. For $E >> D$ treat the collision of the H_2^+ ion as two events consisting of the scattering of proton "A" and proton "B" (impulse approximation). Calculate the differential cross section for proton "A", $\sigma_{H^+}(\theta)$. Calculate the probability, P, that proton "B" is oriented with respect to proton "A" such that $D > \frac{1}{2}\mu(\Delta V)^2$. It then follows that

$$\sigma_{H_2^+}(\theta) = P\,\sigma_{H^+}(\theta). \qquad (1)$$

The electron is not treated as a scattered particle in this model but may be thought of as simply providing the binding energy.

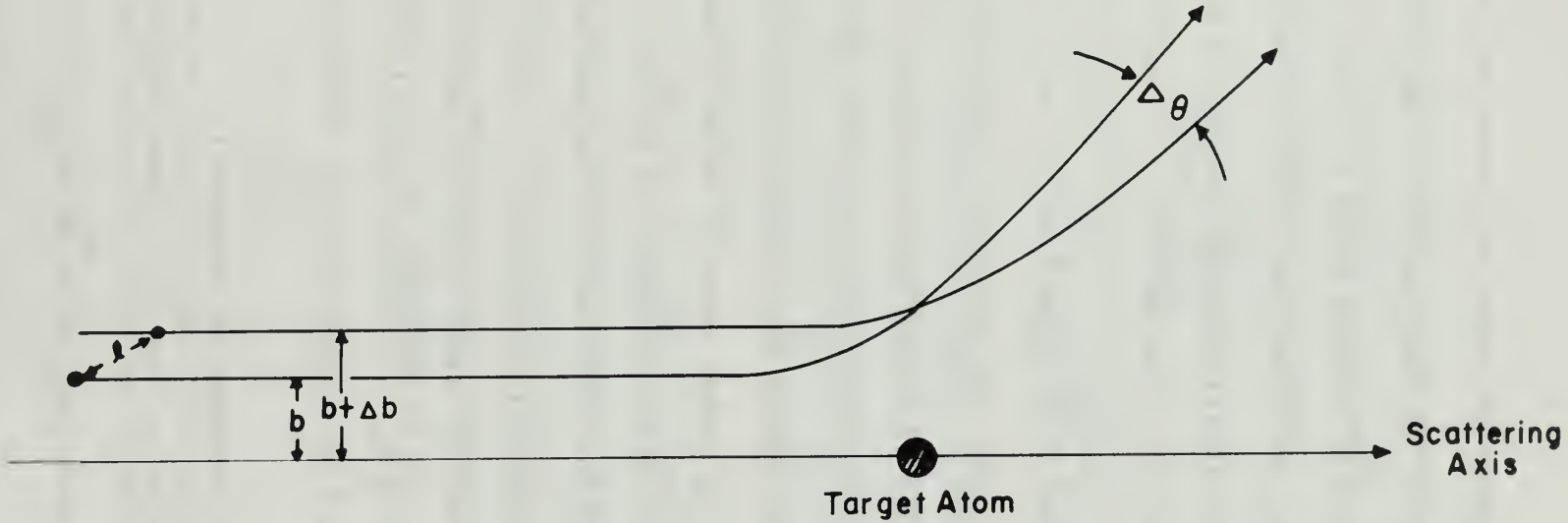

Figure 2. Protons with the same scattering plane but different impact parameters.

B. CALCULATION OF $\sigma_{H^+}(\theta)$

The calculation of $\sigma_{H^+}(\theta)$ was done on an IBM 360-67 digital computer using a program written by Feist [2]. The program utilizes standard numerical techniques to solve the classical differential scattering equations. The potentials used are shielded coulomb potentials from Byatt [3] of the form

$$V(r) = \frac{Ze^2}{r} \left(\sum_n C_n e^{-b_n r}\right)$$

with $\sum_n C_n = 1$ but C_n and b_n otherwise adjustable. Byatt lists two potentials for Argon, one with and one without correction for polarization. The two potentials yielded cross sections for H^+ that were within 13% of each other for an incident energy of 100 eV and scattering angles from 38^o to 50^o (laboratory co-ordinates). Due to the close agreement of the two potentials, only the one corrected for polarization is presented here. Byatt indicates the potentials should be accurate to within 5% for $\sum_n C_n e^{-b_n r} > .01$. For the region where the potentials were used it was noted that $\sum_n C_n e^{-b_n r} > .052$. Thus it was felt that these potentials should be satisfactory for calculating $\sigma_{H^+}(\theta)$.

C. CALCULATION OF THE ORIENTATION PROBABILITY

The energy criterion for the H_2^+ ion remaining intact may be put as

$$D = \frac{\mu}{2} (\Delta V_{max})^2 = \frac{M_p}{4} (\Delta V_{max})^2$$

$$\text{or} \qquad \Delta V_{max} = \left[\frac{4D}{M_p}\right]^{\frac{1}{2}}. \qquad (2)$$

Considering the case where the target mass is much greater than the mass of the H_2^+ ion, the H_2^+ ion has energy after collision $E_o = M_p V_o^2$ both in the laboratory and center of mass systems. Substituting this into equation (2) gives

$$\Delta V_{max} = \left[\frac{4D}{E_o}\right]^{\frac{1}{2}} V_o \ .$$

Now it was shown in Section II A, that $\Delta V_{max} = f(b, \Delta b, \Delta\emptyset)$. Therefore, for a fixed incident energy and impact parameter, there exists a function g such that $\Delta\emptyset = g(\Delta b)$. This defines a closed curve in a plane perpendicular to the scattering axis that proton "B" must pass through in order for the ion to remain intact. The area enclosed by the $\Delta\emptyset = g(\Delta b)$ curve is designated by S.

The axis of the H_2^+ ion is randomly oriented with proton "B" having no preferred position with respect to proton "A". The location of proton "B" will therefore define a sphere about proton "A" of radius ℓ, the internuclear separation. The orientation probability is then given by the ratio of S to one-half the area of this sphere

$$P = \frac{S}{2\pi\ell^2} \ . \qquad (3)$$

The justification for using the area of a hemisphere in the denominator of equation (3) is that the "other half" is redundant. No exact solution has been found for equation (3) and the following approximations were made.

First, it has been assumed that the target is infinitely heavy so that the speed of the H_2^+ ion is unchanged by the collision. For the reaction studied experimentally, this is valid in that $M_{H_2^+} = 2.032$ amu and $M_{Ar} = 39.948$ amu. For example, a 100 eV H_2^+ ion scattered at 45^o has an initial speed of 9.80×10^4 m/sec and a final speed of 9.75×10^4 m/sec. It is further assumed that the two protons will both have this same speed after collision and that disruption will occur due to difference in direction only. Feist [1] showed that the disruptive effect of the difference in the magnitudes of velocities of the two protons is much less than the disruptive effect of their difference in direction. For the case where $\Delta\phi = 0$, and assuming $\Delta\theta$ is small, $\Delta V_{max} = V_o[\Delta\theta_{max}]_{\Delta\phi = 0}$. Using equation (2) this becomes

$$[\Delta\theta_{max}]_{\Delta\phi = 0} = \left[\frac{4D}{E_o}\right]^{\frac{1}{2}} . \qquad (4)$$

Figure 3a illustrates this case. For the case where $\Delta\theta = 0$ (or equivalently $\Delta b = 0$) and assuming $\Delta\phi$ is small, $\Delta V_{max} = V_o \sin\theta\,[\Delta\phi_{max}]_{\Delta b = 0}$. Using equation (2) this becomes

$$[\Delta\phi_{max}]_{\Delta b = 0} = \left[\frac{4D}{E_o}\right]^{\frac{1}{2}} \frac{1}{\sin\theta} . \qquad (5)$$

Figure 3b illustrates this case. Using the classical definition for differential scattering $|2\pi b db| = |\sigma_{H^+}(\theta)\, 2\pi \sin\theta\, d\theta|$, it is seen that

$$|\Delta b_{max}|_{\Delta\phi = 0} = \frac{\sigma_{H^+}(\theta) \sin\theta}{b} \left[\Delta\theta_{max}\right]_{\Delta\phi = 0} ,$$

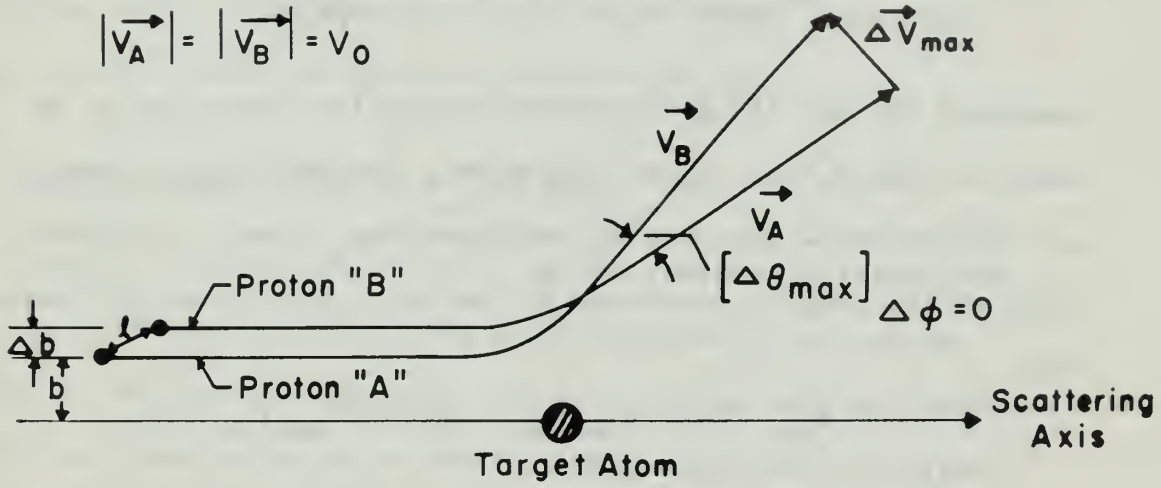

Figure 3.a. Proton velocity difference due to difference in impact parameter.

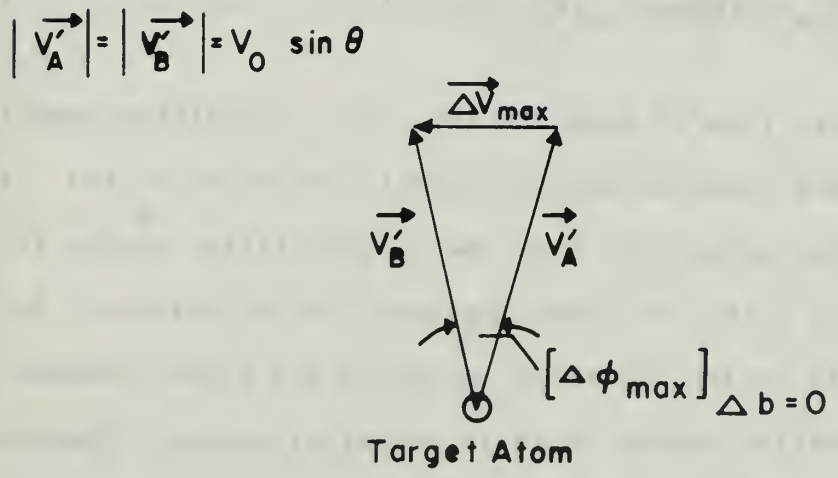

Figure 3. b. Proton velocity difference due to difference in scattering plane.

which, upon combining with equation (4) becomes

$$|\Delta b_{max}|_{\Delta\phi = 0} = \frac{\sigma_{H^+}(\theta) \sin\theta}{b} \left[\frac{4D}{E_o}\right]^{\frac{1}{2}} . \qquad (6)$$

Equations (5) and (6) give maximum values for either Δb or $\Delta\phi$ such that the H_2^+ ion is not disrupted. The $\Delta\phi = g(\Delta b)$ curve must therefore be enclosed by these maximum values. An upper bound on the area, S, enclosed by the $\Delta\phi = g(\Delta b)$ curve is therefore

$$S_{max} = [2(\Delta b_{max})_{\Delta\phi = 0}][2b(\Delta\phi_{max})_{\Delta b = 0}].$$

Substituting equations (5) and (6) into the above and using equation (3) an upper bound on the orientation probability is found to be

$$P_{max} = 8 \frac{D}{E_o} \frac{\sigma_{H^+}(\theta)}{\pi \ell^2} \qquad (7)$$

$$\text{and} \quad \left[\sigma_{H_2^+}(\theta)\right]_{max} = \frac{8D}{\pi \ell^2 E_o} [\sigma_{H^+}(\theta)]^2 . \qquad (8)$$

Due to the simple form of equation (8), it is calculated numerically in the same computer program used to calculate $\sigma_{H^+}(\theta)$. It should be further noted that D is the disassociation energy for ground state and ℓ the corresponding equilibrium distance. Excited electronic states for the H_2^+ molecule are either unbound or have very shallow minima in their potential curves. Therefore, if the H_2^+ ion is excited to higher electronic states during the collision process it is almost certain to be disrupted due to

velocity differences after the collision. If the H_2^+ ion is excited to higher vibrational levels, then D would be decreased and ℓ increased. The molecule could still remain intact but would have a smaller value of P and hence $\sigma_{H_2^+}(\theta)$.

D. COMPUTER CALCULATION OF $\sigma_{H^+}(\theta)$ AND $\sigma_{H_2^+}(\theta)$

Figure 4 displays the results of the computer calculations for the differential scattering cross sections. One set of curves is for the $\underline{H^+}$ + Ar → $\underline{H^+}$ + Ar reaction at incident energies of 100,300, and 500 electron-volts. The second set of curves is for the $\underline{H_2^+}$ + Ar → $\underline{H_2^+}$ + Ar reaction also at incident energies of 100, 300, and 500 electron-volts. The H_2^+ curves were computed using equation (8) and represent a predicted upper limit on the scattering cross section.

It is noted that all of the curves are monotonically decreasing functions of scattering angle and reflect no atomic structure.

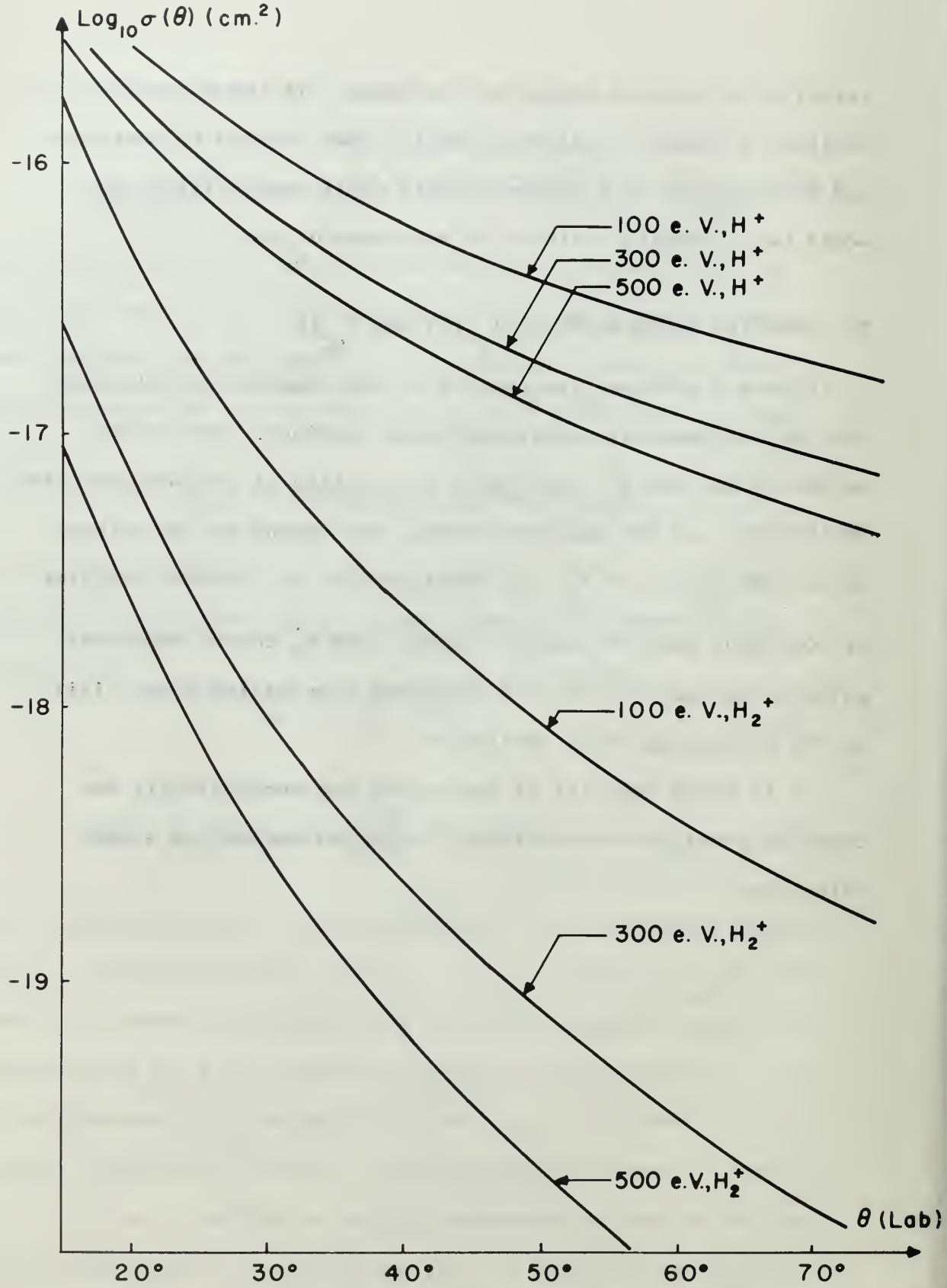

Figure 4. Log of scattering cross section vs. scattering angle for $H^+ + Ar \rightarrow H^+ + Ar$ and $H_2^+ + Ar \rightarrow H_2^+ + Ar$.

III. EXPERIMENTAL APPARATUS

A. GENERAL DESCRIPTION.

The experimental apparatus used to measure the cross sections for the $\underline{H}^+$, $\underline{H_2^+}$ + Ar → $\underline{H}^+$, $\underline{H_2^+}$ + Ar reactions is discussed in detail by Bush [4]. An overall schematic of the apparatus is shown in Fig. 5. The operation of the apparatus was as follows. Three species of hydrogen ions (H^+, H_2^+, H_3^+) were produced in the duoplasmatron ion source and were accelerated electrostatically to the desired energy. The ions entered a mass analyzer where the desired ion species was bent through a 45^o angle to travel down the geometric axis of the apparatus. The selected beam was focused and entered the scattering cell where the target gas, in this case Argon, was contained. The scattering cell was centered in a large focusing magnet that produced a known non-uniform but axially symmetric magnetic field. The trajectory of an ion with a given vector momentum could then be calculated and the detector was appropriately placed to collect this ion. Due to the finite detector size, ions scattered within a finite $\Delta\theta$ (on the order of 1^o) were also detected. It is further noted that essentially all the ions scattered at an angle θ were collected regardless of their azimuthal angle of departure. Cross section measurements at different scattering angles could be made in two ways. Either the detector could be fixed on the magnetic/geometric axis and the focusing magnet current varied to select

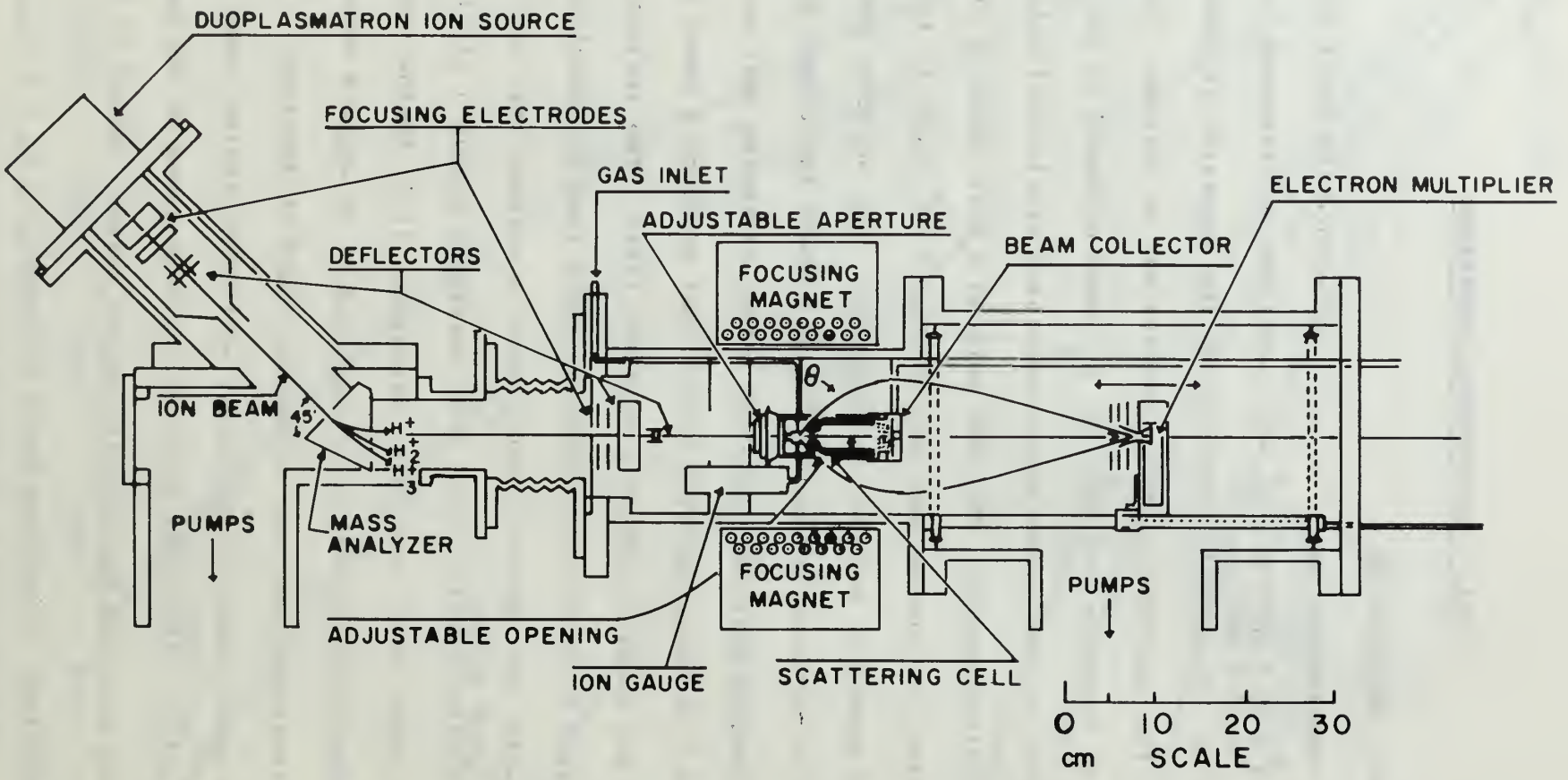

FIGURE 5. SCHEMATIC OF THE EXPERIMENTAL APPARATUS.

the desired scattering angles, or the focusing magnet current could be fixed and the detector moved along the magnetic/geometric axis to select the desired scattering angles. In this experiment, the latter method was used. The detector system consisted of a magnetic electron multiplier whose output was fed into an electrometer. The entire system was maintained at a vacuum on the order of 10^{-5} torr during operation by two diffusion pumps.

B. THE DUOPLASMATRON ION SOURCE.

The duoplasmatron ion source was constructed and described in detail by Carter [5]. Figures 6 and 7 display the construction of the source and the circuit diagram for its operation. The operation of the source basically consisted of maintaining the plasma discharge in the Z-electrode cavity and extracting ions at the desired energy by placing this potential on the anode. Focusing the extracted beam was accomplished by an electro-magnet surrounding the Z-electrode cavity and a conventional Einzel lens and deflector stack.

To increase the beam intensity an acceleration-deceleration system was utilized. This consisted of extending the extraction lens, L_1, to enclose the entire focusing stack. This enclosure was called the "sock". (See Fig. 7.) By floating the sock at a negative potential V (typically -500 volts) and by increasing the potentials of the interior lenses and deflectors by the same amount, the extracted ions transversed this region with an energy

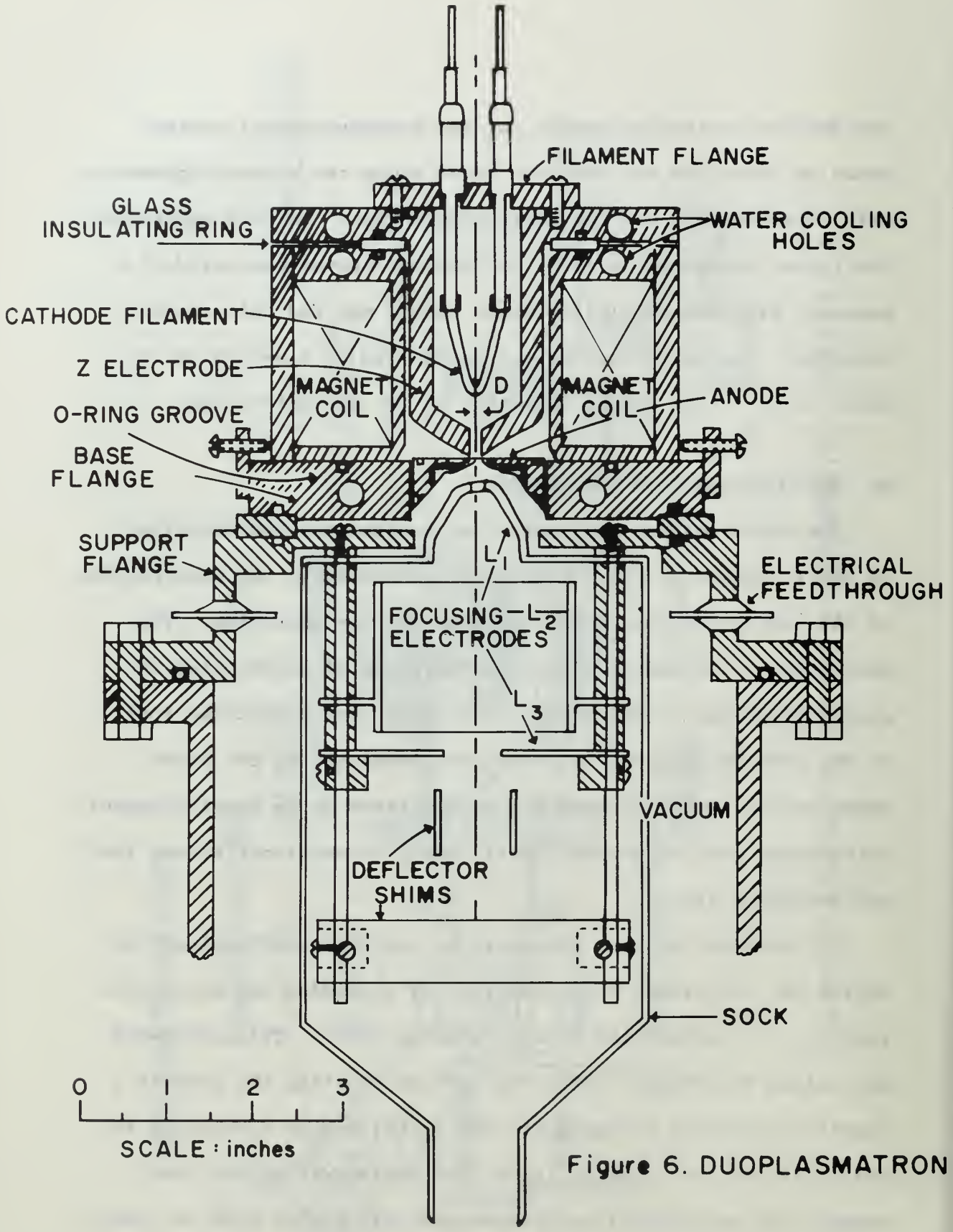

Figure 6. DUOPLASMATRON

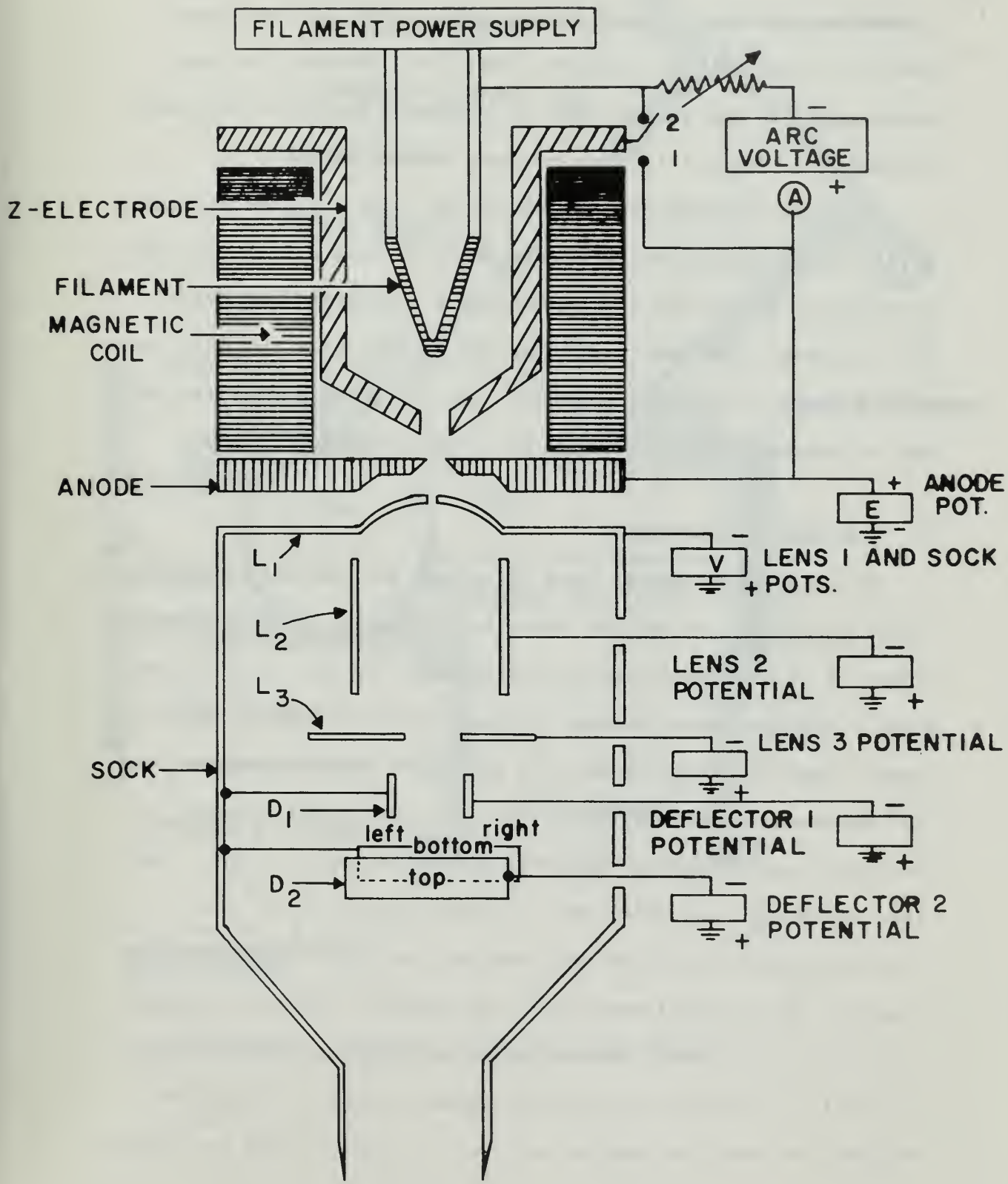

FIGURE 7.
CIRCUIT DIAGRAM FOR DUOPLASMATRON

(E + V)e, yielding a higher space charge limit for the beam density. Upon exiting from the sock, the hydrogen ions were decelerated to energy Ee. This arrangement increased the beam intensity at the scattering cell by a factor of about 40.

A typical maximum beam intensity for mass analyzed protons of 100 eV delivered to the scattering cell with 0.5 cm entrance aperture at 80 cm from the source was 1×10^{-7} amperes. For H_2^+ ions under the same conditions the maximum beam intensity was on the order of 2×10^{-7} amperes. The energy spread of the beam was estimated to be about 2 eV for a 100 eV beam.

C. THE MASS SPECTROMETER.

The mass spectrometer used to select the desired ion was constructed, calibrated and described in detail by Strohsahl [6]. Figure 8 is a schematic of its arrangement in the overall apparatus. The mass spectrometer utilized an electromagnet to produce a magnetic field of up to 4 kilogauss confined between two 40° wedge-shaped pole pieces. This was sufficient to mass analyze atomic masses up to 40 with energies up to 1 KeV. The resolution $(\frac{m}{\Delta m})$ was about 40. A bending angle of 45° was utilized and this altered the selected ion beam trajectory from the axis of the duoplasmatron to the geometric axis of the main scattering apparatus. Operation of the mass analyzer consisted of merely of setting the correct magnet current to focus the desired ion into the scattering cell. The pole faces and region

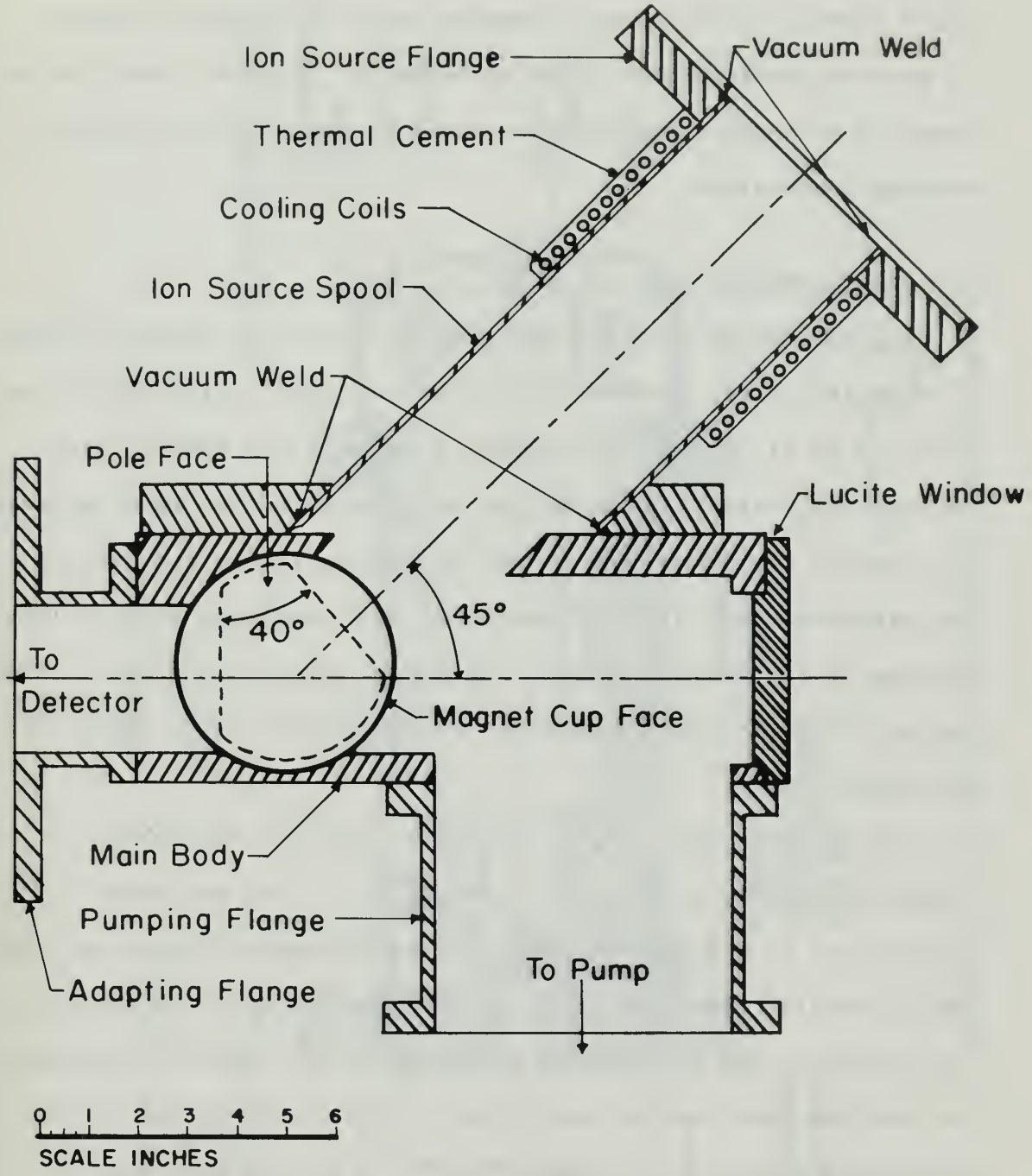

Figure 8. Schematic of Mass Spectrometer.

where undesired species were "dumped" were coated with aquadag to prevent static charges from building up. Even so, this region required thorough cleaning after about 20 hours of duoplasmatron-analyzer operations.

D. THE SCATTERING CELL.

The scattering cell was designed by Bush [4]. Figure 9 shows a schematic of its construction. The functions of the scattering cell are to (1) allow the collimated incident ion beam to pass through the scattering region and be measured by the beam collector, (2) contain the target gas in the scattering region and measure its pressure, and (3) allow scattered ions to escape over as large a range of scattering angle and azimuthal angle as possible. The design of the scattering cell was a compromise between these requirements.

The incident beam enters the scattering cell through an adjustable aperture (diameter from 0.1 to 1.0 cm) which was usually set at 0.5 cm. The beam passed through the front section which contains the scattering region. Now the great majority of the incident ions will not be scattered at all and will continue on into the rear section where they are collected either by the rear section wall or the beam collector. The incident beam was measured by two Keithly Model 410 Micro-Microammeters. The beam collector, which collects about 90% of the beam, had three grids that prevented slow ions from being collected and suppressed secondary electron emission. The beam collector assembly could be swung off axis allowing a clear path through the scattering cell for system alignment and detector calibration.

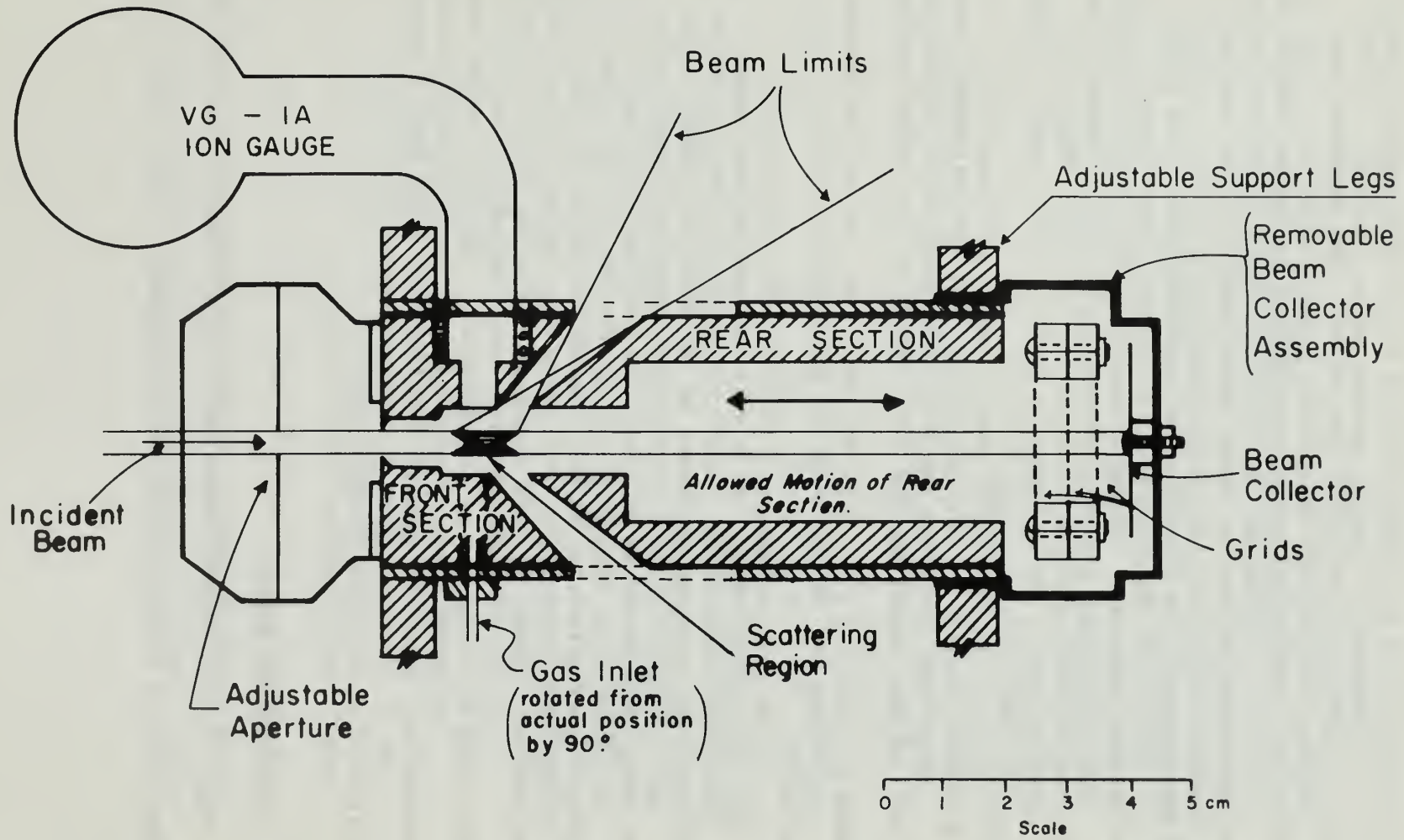

Figure 9. The Scattering Cell and Beam Collector

The target gas was bled into the scattering region through a Granville-Phillips variable leak valve. The pressure was measured by a VG-1A ion gauge manufactured by Vacuum Industries. Since operation of the ion gauge interfered with the incident beam measurement, the pressure was measured before and after each run and averaged. Vacuum Industries lists the correction factor for Argon (relative to dry air) as 0.617. That is, $P_{actual} = 0.617 \times P_{indicated}$.

The rear section of the scattering cell was adjustable along the axis of the apparatus and thus regulated the target thickness between 0.1 and 0.8 cm. This was set at 0.3 cm for the present experiment.

The scattering angle limits were defined by the slope of the front and rear section shoulders of 49^{o} and 36^{o} respectively. This range of scattering angles could be extended somewhat by considering an effective target thickness. Bush [4] describes this process. Ideally, ions scattered into all 360^{o} of azimuthal angle could be collected at the detector. However, interference by mechanical support required for the scattering cell reduced the available azimuthal angle to 290^{o}.

E. THE FOCUSING MAGNET.

The focusing magnet consisted of five concentric spools of copper wire in a parallel-series arrangement. Each spool was

water-cooled by a ¼ inch copper tubing jacket. A Sorenson Nobatron DCR 150-15 power supply maintained the desired current setting for periods of several hours with essentially no drift.

The magnetic field on the center axis was carefully surveyed by Kelly [7] using a Hall probe. Figure 10 shows the result of these measurements. Kelly also showed that the magnetic field was symmetric about the coil axis to within 0.1%. This allowed the axis of the apparatus to be aligned with the coil axis so that the magnetic axis coincided with the geometric apparatus axis.

In order to better understand the function of the focusing magnet, it is instructive to consider the simpler case of a uniform axially symmetric magnetic field. This would correspond to the entire apparatus being enclosed in a long solenoid. For an ion of charge q with momentum p and scattered at an angle θ the trajectory is a helix such that after one orbital revolution the ion will again intercept the axis at some distance Z_o. Using these boundary conditions the Lorenz force equation $\vec{F} = q\,\vec{v} \times \vec{B}$ can be integrated to give $Z_o = \frac{2\pi}{qB} p \cos\theta$. A detector placed at Z_o will then detect the scattered ion. (See Fig. 11.) This equation also shows the two ways of detecting scattered ions over a range of θ and p. Either maintain B constant and vary the detector position or keep the detector fixed and vary B.

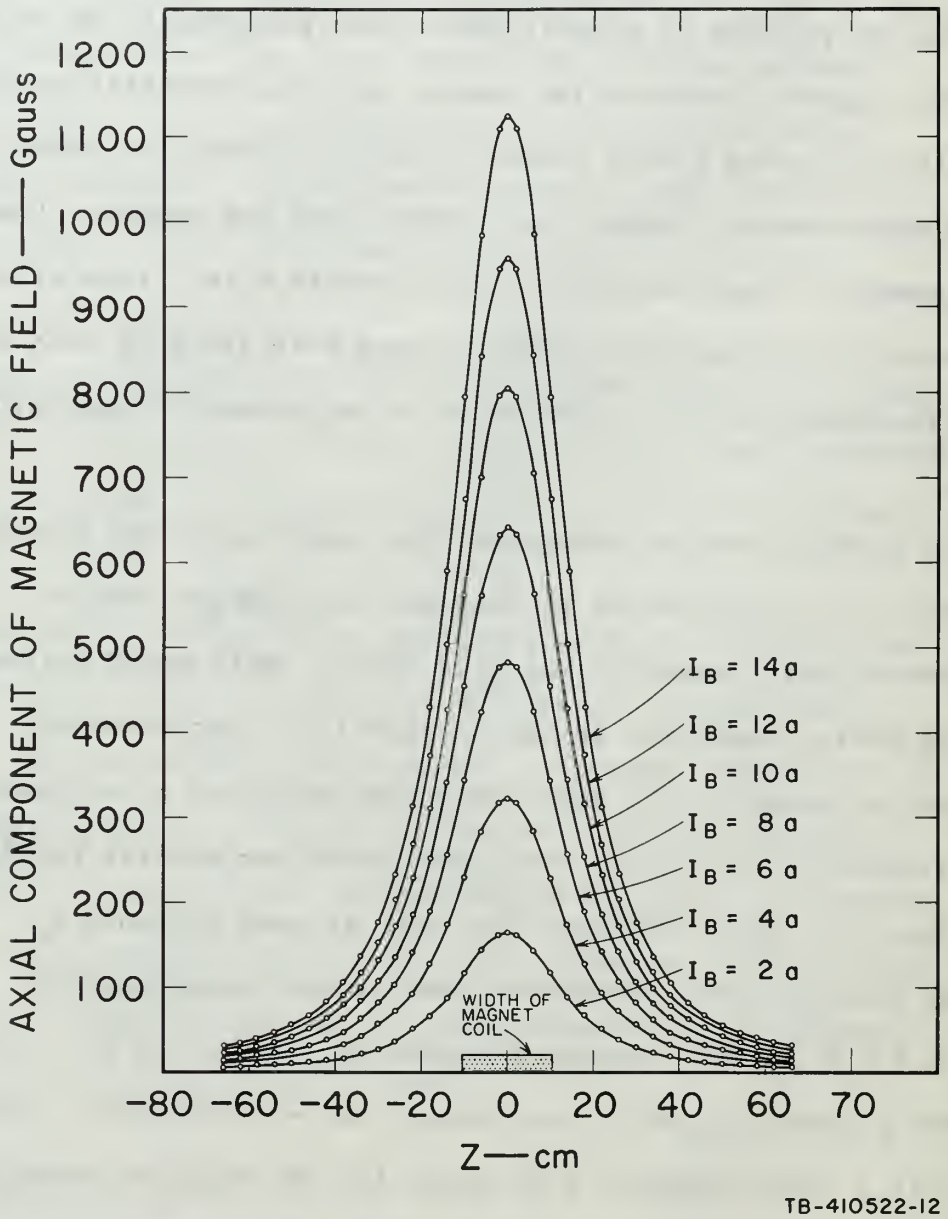

Figure 10. Magnetic Field Strength at Various Distances Along the Magnetic Axis for Various Currents

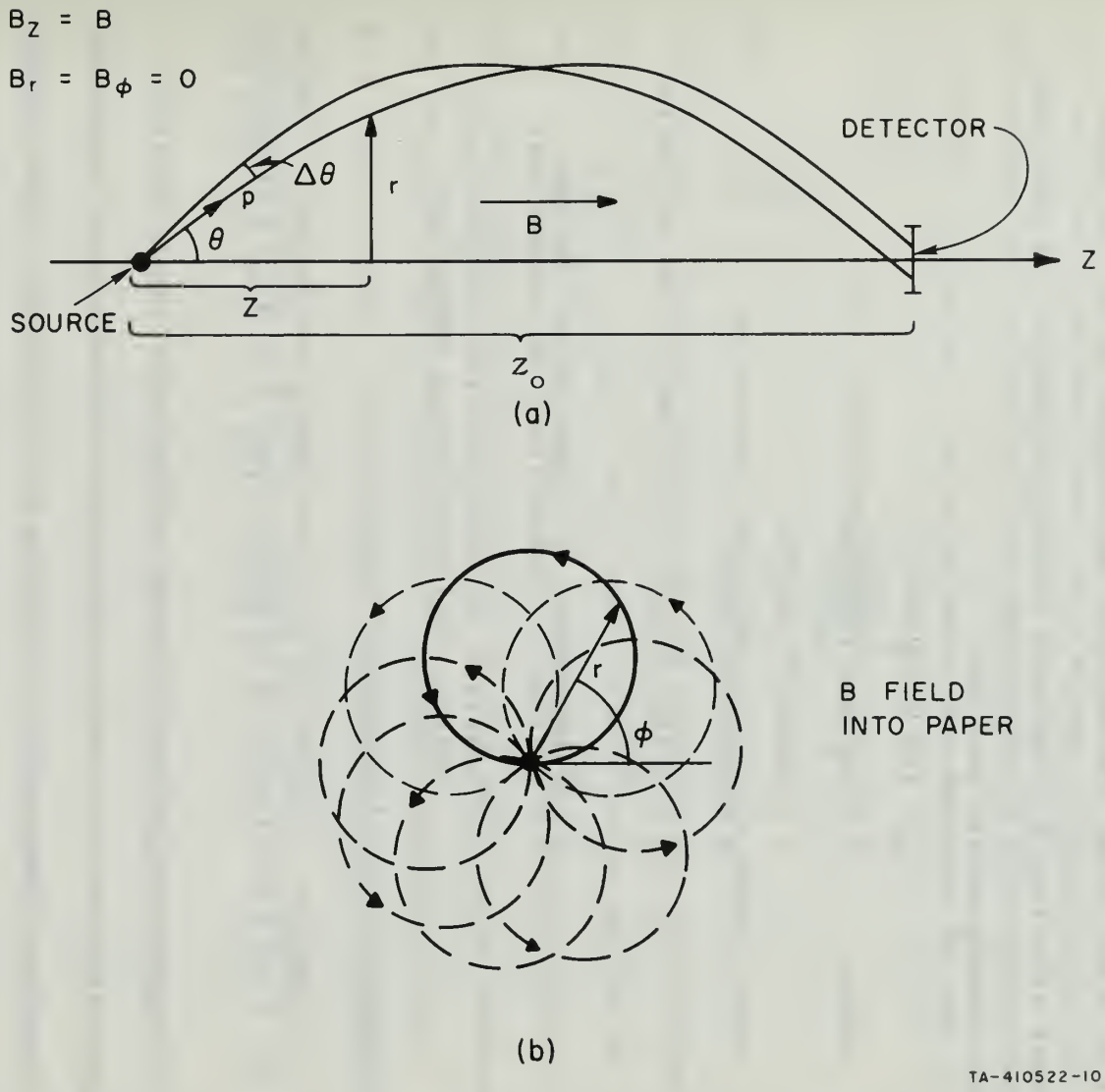

Figure 11. Orbit of Charged Particle in Uniform Magnetic Field

Now in order to measure a differential scattering cross section, the solid angle that the finite size detector "sees" must be known. For the axially symmetric case this is $d\Omega = 2\pi \sin\theta \, d\theta$. To evaluate $d\theta$ consider the various parameters affecting Z_o, the axis intercept distance. A functional relationship exists such that:

$$Z_o = f(E,\theta,B,\rho,\eta,C)$$

where

E = energy of incident ion

θ = angle of scatter

B = magnetic field

ρ = radial target displacement from the system axis

η = displacement of target atom from the scattering center along the system axis

C = constant for each reaction including mass ratios, inelastic energy losses, etc.

Differentiating this expression gives

$$\Delta Z_o = \left(\frac{\partial Z_o}{\partial E}\right)\Delta E + \left(\frac{\partial Z_o}{\partial \theta}\right)\Delta\theta + \left(\frac{\partial Z_o}{\partial B}\right)\Delta B + \left(\frac{\partial Z_o}{\partial \rho}\right)\Delta\rho + \left(\frac{\partial Z_o}{\partial \eta}\right)\Delta\eta + \left(\frac{\partial Z_o}{\partial C}\right)\Delta C$$

For a specific measurement ΔB and ΔC are zero. Since analytic expressions for the various derivatives are not known, they must be evaluated numerically by varying E, θ, ρ, and η. Bush, Cook, Heinz, and Rodeback [8] estimate that $\Delta\rho$ and $\Delta\eta$ which are due to the finite volume of the scattering region affect $\Delta\theta$ by no more than 10%. Approximating $\Delta\rho$ and $\Delta\eta$ as zero the above expression can be rearranged to $\Delta\theta = \left(\frac{\partial\theta}{\partial Z_o}\right)\left[\Delta Z_o - \left(\frac{\partial Z_o}{\partial E}\right)\Delta E\right]$.

The effect of a small (2%) energy spread was studied and it was concluded that the "effective" $\Delta\theta$ was not changed. The angular resolution of the apparatus was degraded somewhat in that not all particles scattered within $\Delta\theta$ of θ were collected but this was compensated by the fact that some particles scattered outside of $\Delta\theta$ were collected. The solid angle can therefore be approximated as

$$d\Omega \simeq 2\pi \sin\theta \left| \left(\frac{\partial\theta}{\partial z_o} \right) \right| \Delta z_o$$

where $\pm \frac{\Delta z_o}{2}$ is the maximum deviation of the trajectory intercept from z_o that will still allow the particle to be collected by the detector. Δz_o can be calculated by considering the detector geometry and the angle θ_o with which the particle intercepts the Z-axis. As an example of how the approximate expression for the solid angle is applied if an analytic expression for $z_o = f(\theta)$ is known, consider again the uniform axially symmetric magnetic field. Recalling that $z_o = \frac{2\pi}{qB} \cos\theta$, it follows that $d\Omega \simeq \frac{qB}{p} \Delta z_o$.

For the non-uniform axially symmetric field, the procedure for computing trajectories and solid angles was essentially the same as for the uniform case except that the calculations were done numerically on an IBM 360-67 digital computer. The program that accomplished this is explained in Appendix A. A very brief outline of the program is as follows.

(1) Express the magnetic field along the axis as a 12th order polinomial. This gives $B_z = (I) \sum_{1}^{13} C_n Z^{n-1}$ where I is the magnet current.

(2) Using this polynomial, a vector potential is found.

(3) Combining the vector potential with the Lorentz force equation gives a 2nd order non-linear differential equation. This is expressed as two simultaneous, first-order differential equations which are integrated by the DHPGC Subroutine of the Scientific Subroutine Package for the IBM 360-67 computer. The trajectory, Z_o, and Θ_o are now known.

(4) The above procedure is done over a selected range of scattering angles and a polynomial expressing $\Theta = f(Z_o)$ is generated.

(5) From Θ_o and the detector geometry, ΔZ_o is calculated.

(6) The solid angle can now be calculated as $d\Omega(\Theta) = 2\pi \left(\frac{290}{360}\right) \sin\Theta \left(\frac{\partial\Theta}{\partial Z_o}\right) \Delta Z_o$. The factor $\left(\frac{290}{360}\right)$ is present due to the construction of the scattering cell.

Figure 12 shows a series of trajectories computed for H^+ ions with incident energy of 100 eV elastically scattered by Argon.

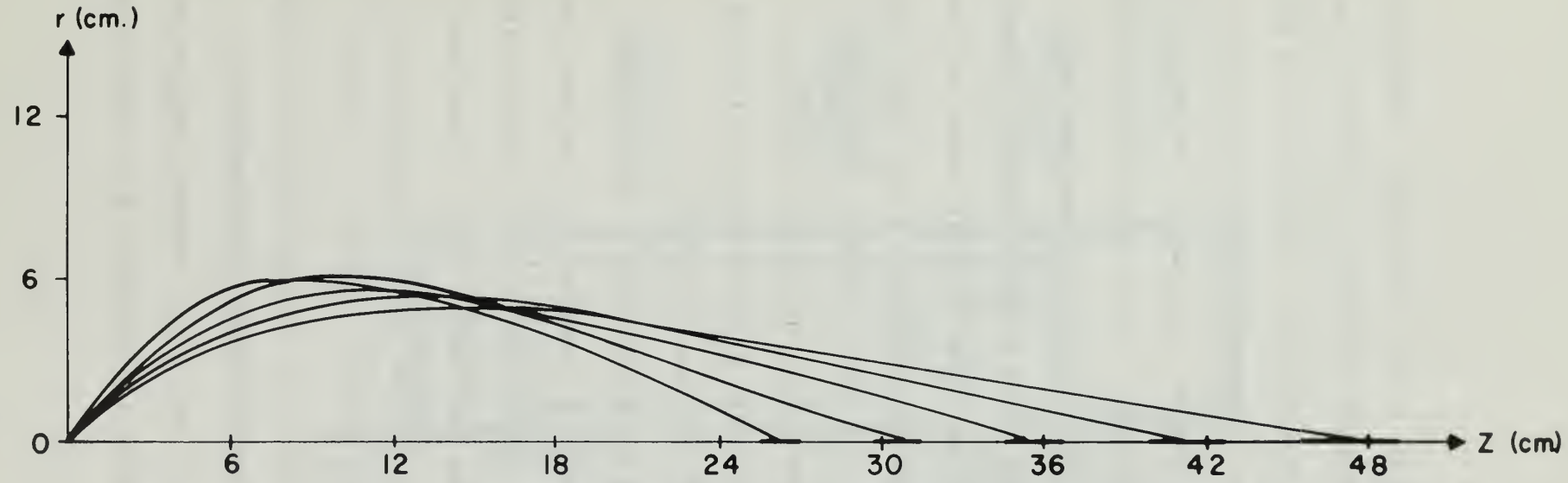

θ scatter	52°	48°	44°	40°	36°
Z_o	26.3	30.7	35.5	41.2	47.5
ΔZ_o	1.2	1.7	2.3	2.9	3.7
θ_o	23.2°	18.9°	15.3°	12.2°	9.6°
$d\Omega$	.078	.098	.108	.110	.113

Figure 12. Trajectories of H^+ Ions, with 100 eV. Incident energy scattered by argon, in focusing magnetic field with I = 4.8 amps.

F. THE DETECTOR.

The detector system employed in this experiment consisted of a Bendix Model 306 Magnetic Electron Multiplier (MEM) which was fed into a Keithly Model 640 Electrometer. Figures 13, 14 and 15 show the detector geometry, a schematic of operation, and a circuit diagram. The principle of operation of the multiplier was as follows. An incident ion was accelerated to about 1500 eV and ejected an electron from the tungsten cathode upon impact. A crossed electric and magnetic field (alnico permanent magnets) imparted a cyclical trajectory to the electron(s) down the dynode strip. The glass dynode and field strips had a high resistance coating of tin oxide and antimony that sustained the electric field. Each time the electrons struck the dynode strip multiplications occurred so that when the electrons were collected by the anode, a gain of about 10^4 had been realized.

Unfortunately the MEM had to be operated in the focusing magnetic field. This resulted in a sideways drift of the electrons moving down the dynode strip so that all of the electrons generated were not collected at the anode. This in fact made the MEM gain a very sensitive function of its position in the focusing magnetic field. The procedure used was to calibrate the MEM under the same environment that existed during the actual cross section measurements. Specifically, this consisted of: (1) measuring the gain using H_2^+ ions with a focusing magnet current of 6.6 amperes with the detector position, Z_o, varied from

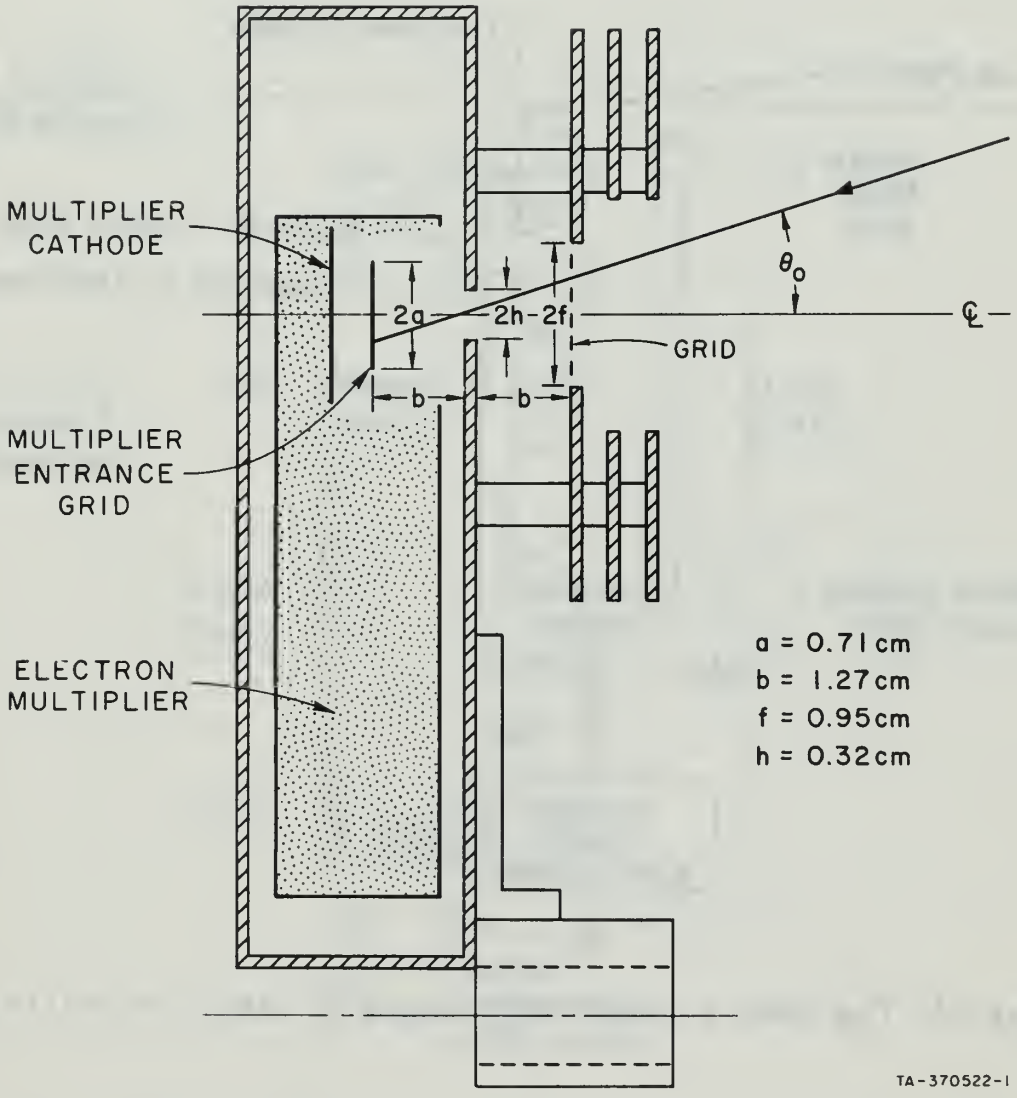

Figure 13. Dector Aperature Geometry.

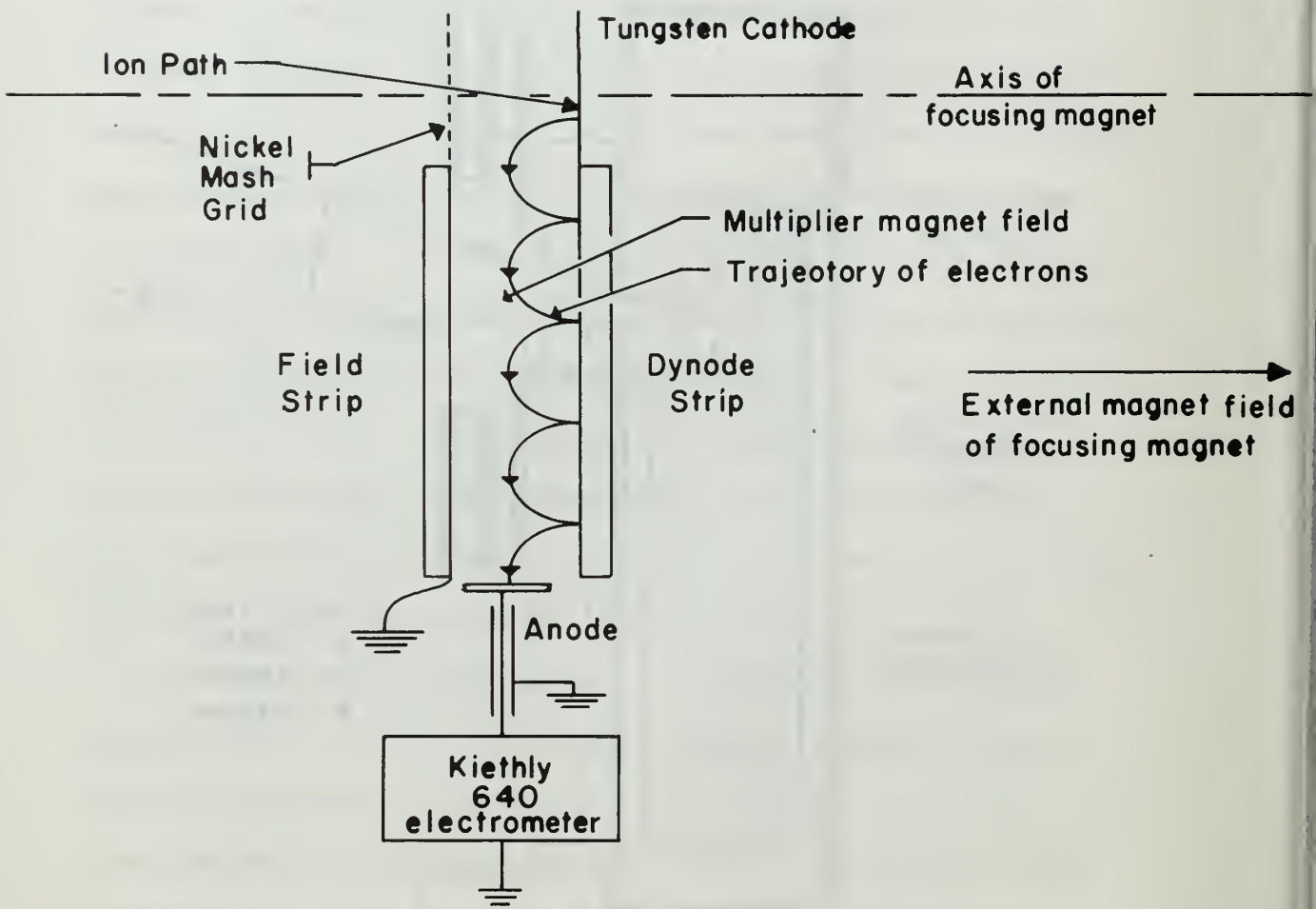

Figure 14. The bendix model 306 magnetic electron multiplier

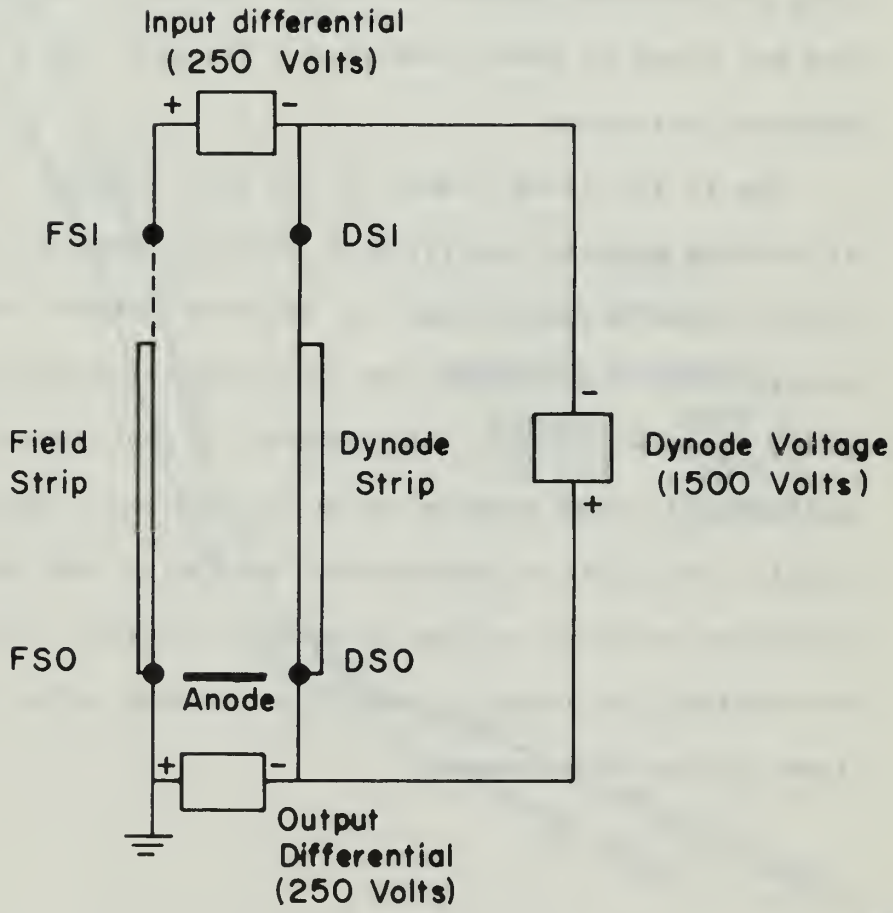

Figure 15. Circuit Diagram for Electron Multiplier.

30.5 to 47.5 centimeters from the scattering cell, (2) measuring the gain using H^+ ions with a focusing magnet current of 4.8 amperes with the detector position, Z_o, varied from 28.5 to 42.5 centimeters from the scattering cell. Since the focusing magnetic field was a known function of current and position, the two gains are plotted against magnetic field in Fig. 16. The gain for H_2^+ ions was measured before and after the cross section measurements and was found to remain constant. The gain for H^+ ions was measured only once.

Due to the steep slopes of the gain curves, a small error in setting detector position or focusing magnet current will result in a large error in the detector current reading. This, coupled with the tedious task of calibrating the detector for every species, energy, and magnetic current that a cross section measurement is to be made, made this detector system less than ideal. For further experimental work with this apparatus, a different detector system is being considered. This may consist of counting the output pulses from the MEM rather than integrating them with an electrometer.

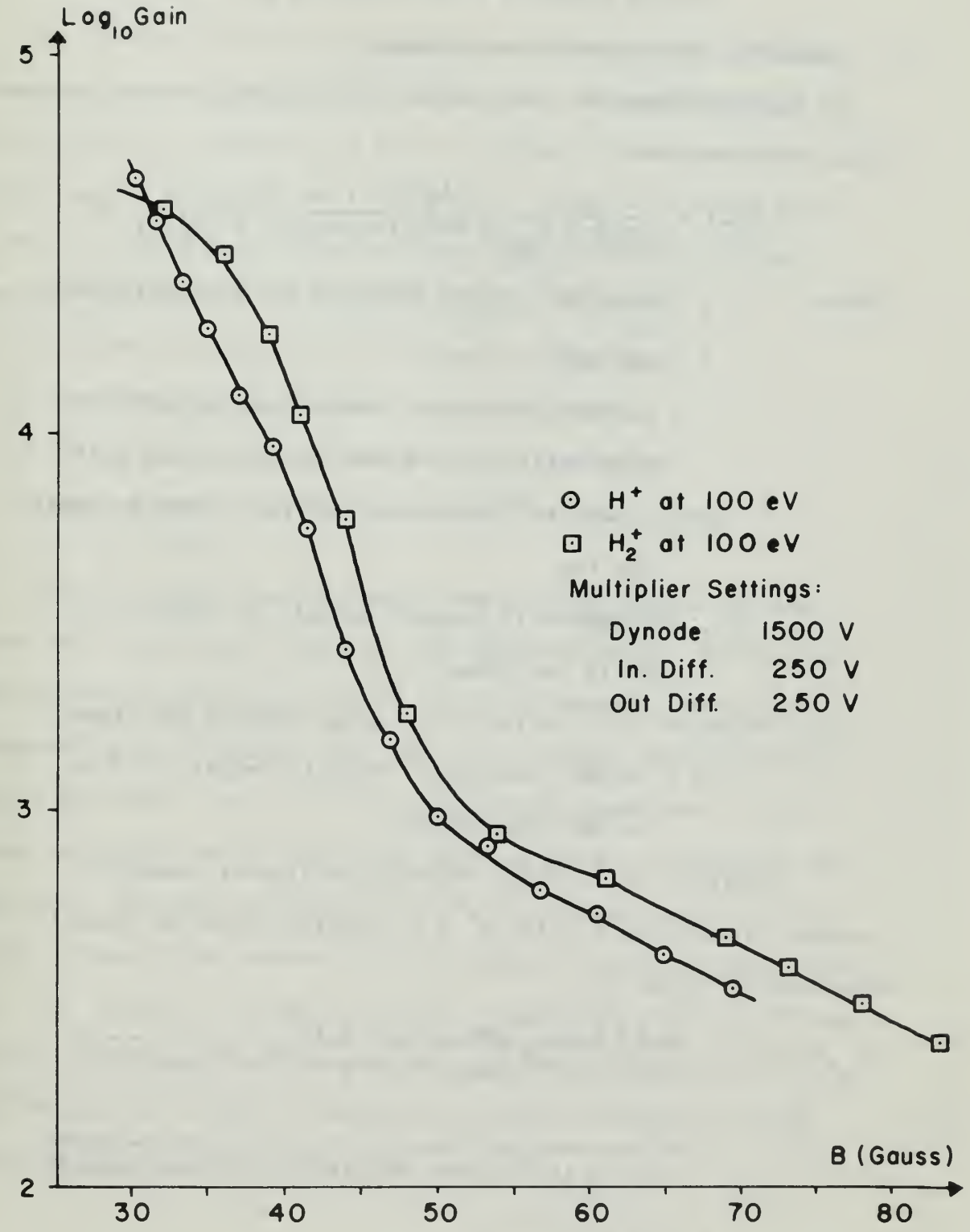

Figure 16. Multiplier gain vs. magnetic field.

IV. EXPERIMENTAL RESULTS

A. LABORATORY CROSS SECTION MEASUREMENT.

The equation used for calculating a differential cross section in the laboratory was

$$d\sigma(\theta) = \frac{I_D/G}{I_i \times (\rho \times P_{sc} \times \text{Corr.Factor}) \times t \times d\Omega(\theta)} \text{ cm}^2.$$

where I_D = detector current measured by an electrometer

G = MEM gain

I_i = Incident ion beam. Sum of the currents to Beam Collector and Rear of Scattering cell.

ρ = 3.54×10^{16} particles/cm^3-torr based on ideal gas law.

P_{sc} = Pressure in scattering cell as measured by VG-1A ion gauge

Corr. Factor = .617; corrects ion gauge reading for Argon

t = target thickness. Normally equal to .3 cm in this experiment

$d\Omega(\theta)$ = Solid angle computed by digital computer.

A sample calculation for the $\underline{H}^+$ + Ar reaction showing typical experimental values is

$$\sigma_{H^+}(41.9^o) = \frac{(1.85 \times 10^{-9} \text{ amp.})/1.27 \times 10^4}{(1.41 \times 10^{-8} \text{ amp.})(3.54 \times 10^{16} \text{cm}^{-3}\text{-torr}^{-1})} \times$$

$$\frac{1}{(1.38 \times 10^{-3} \text{torr} \times .617)(0.3 \text{ cm})(0.109 \text{ sterad})}$$

$$= 1.07 \times 10^{-17} \text{ cm}^2$$

B. MEASUREMENT OF THE $\underline{H}^+ + Ar \rightarrow \underline{H}^+ + Ar$ CROSS SECTION.

The differential scattering cross section for this reaction was measured from 39.2^o to 50^o. Five runs were made and the data points are displayed in Fig. 17 along with the computed cross section using the Byatt potential. Figure 18 shows the average of the 5 runs along with the computed cross section. Important parameters for the measurements included:

(1) Incident energy of H^+ ions equal to 100 eV.

(2) Focusing magnet current equal to 4.8 amps.

(3) Solid angle typically equal to 0.1 steradians.

(4) Argon pressure in scattering cell typically equal to 1×10^{-3} torr.

Figure 18 shows that the experimental curve, while having about the same overall slope as the computed curves, differs in magnitude by a factor of about 6. This difference, while not catastrophic, was greater than expected. First, there may have been a systematic error in the experimental apparatus. A possible systematic error could have been an error in measuring the MEM gain. The gain was measured with an incident beam several orders of magnitude greater than the beam of scattered particles. Thus, if the MEM gain were a (slowly) increasing function of input current, the measured gain would be greater than the gain for the smaller beam of scattered particles. This would result in the measured cross sections being too small.

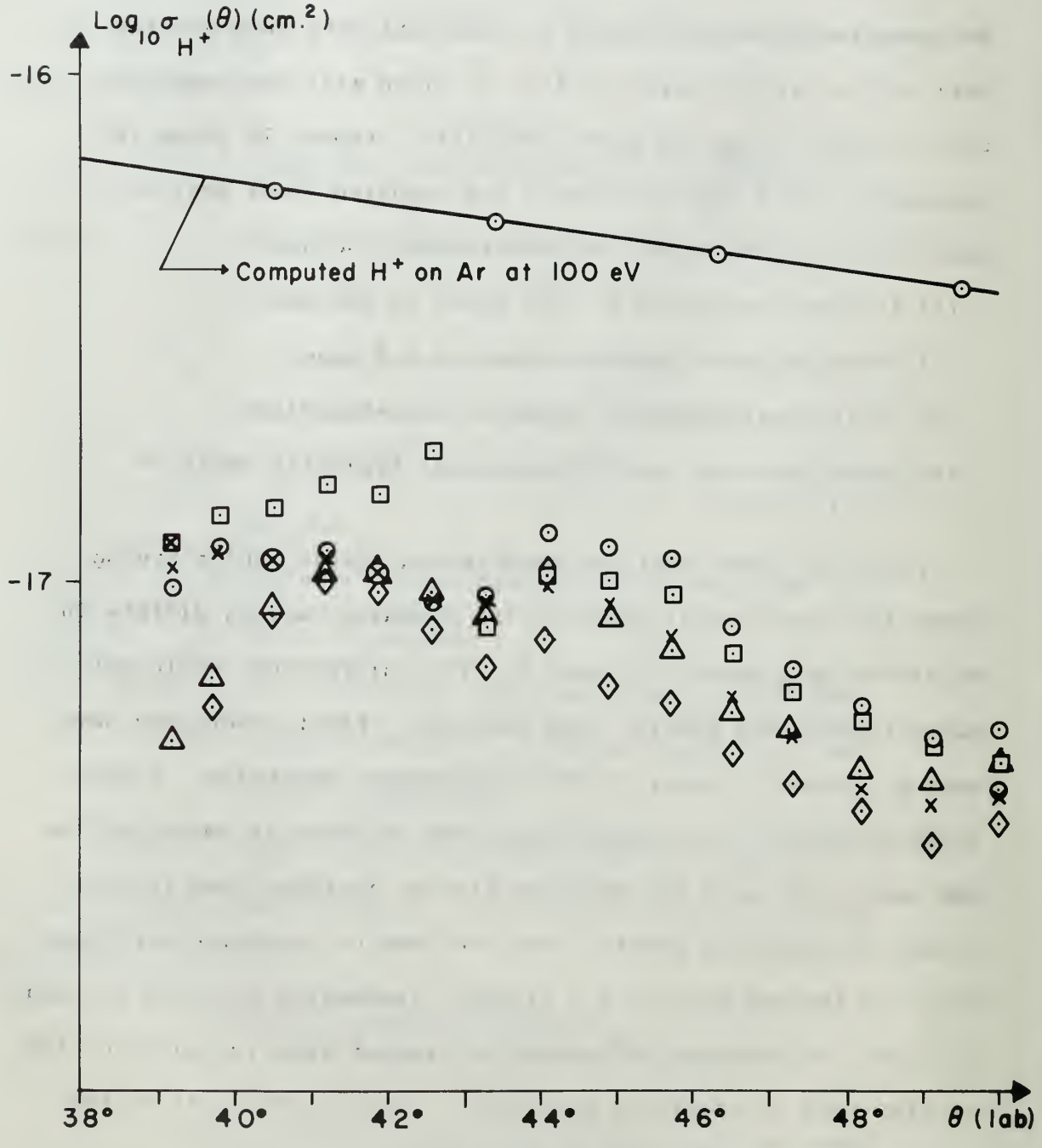

Figure 17. Experimental measurements of $\underline{H}^+ + Ar \rightarrow \underline{H}^+ + Ar$ at 100 eV.

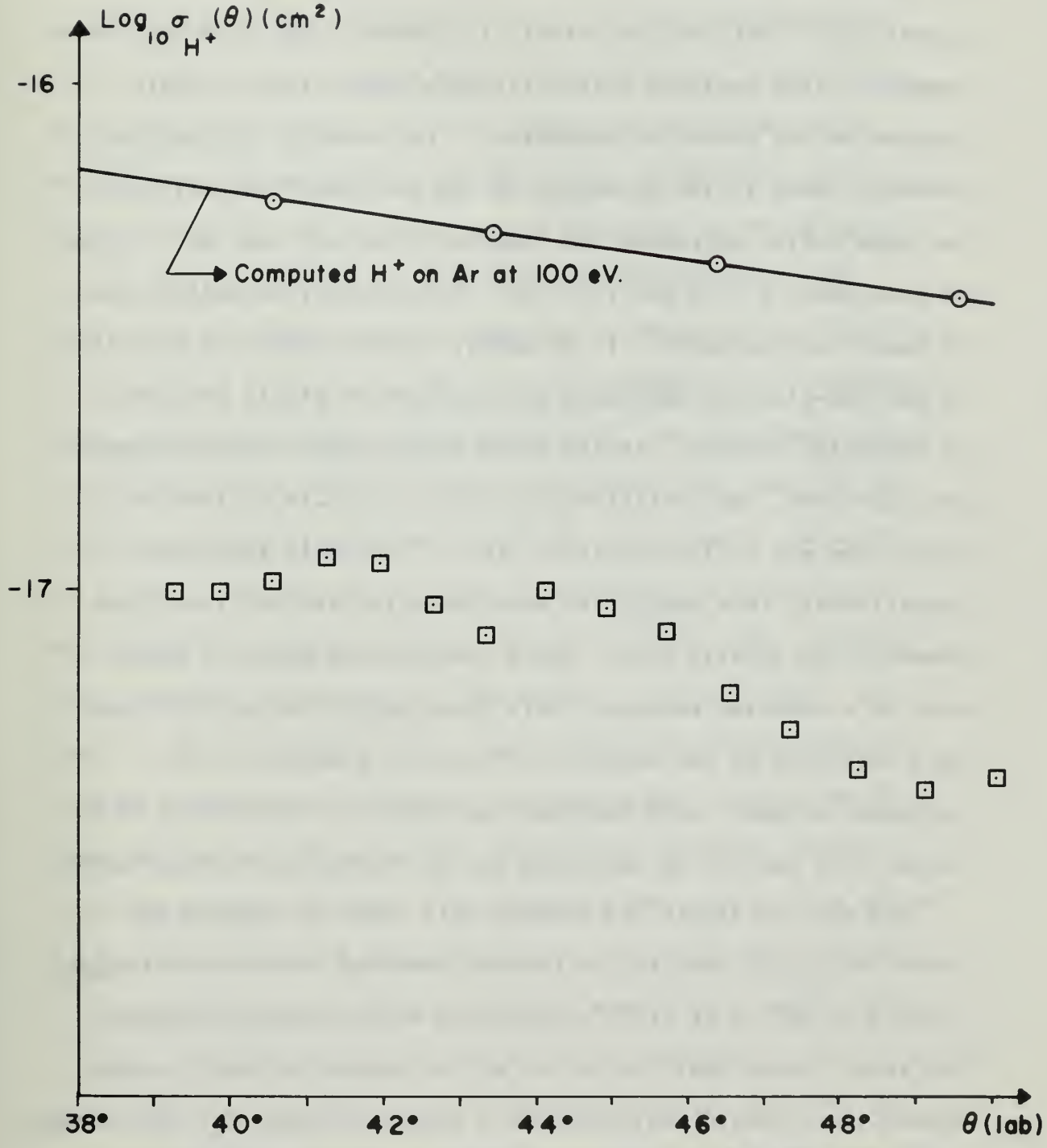

Figure 18. Average of experimental measurements of $\underline{H^+} + Ar \rightarrow \underline{H^+} + Ar$ at 100eV.

Second, the potential may have been inadequate for this application. Varying the potential parameters revealed that the computed cross sections were relatively insensitive to small changes in the potential parameters. For example, varying the dominate terms in the potential by 30% such that the collision was made softer decreased the computed cross sections by a factor of only about 2. It was felt that the potential parameters were at least this accurate. It is noted, however, that the potential is Hartree-like and therefore will reflect no atomic structure or inelastic process. At the large angles where this experiment was conducted, the collisions are relatively hard so that the Argon atom may well be excited. The H^+ ion would then have significantly less energy and momentum after the collision compared to the elastic case. Since the focusing magnetic field acts as a momentum analyzer, only elastically scattered H^+ ions were collected by the detector. Thus, the presence of an inelastic process could decrease the elastic cross section by a factor of 6 and not be accounted for in the Hartree-like potential.

The work of Aberth and Lorents [11] tends to support the second analysis. Aberth and Lorents measured the scattered signal profile of He^+ on Ar at 10^o and 400 eV with an energy analyzer. The result shows that for He^+ on Ar, an inelastic event is more likely than elastic scattering by a factor of about $2\frac{1}{2}$. The energy lost by He^+ in inelastic events was on the order of 10 to 15 eV.

Applying this to the case of H^+ on Ar, it seems reasonable to expect protons to be a more efficient projectile for exciting Ar than He^+ and therefore could account for the factor of 6. Furthermore, inelastically scatter protons with energy after collision of 85 - 90 eV would not be collected by the detector.

The choice between the computed and experimental cross sections was accomplished by comparing the data in Fig. 18 with data supplied by Magnuson, Carlston, and Snyder [9]. Magnuson et al also measured the cross section of H^+ on Ar although their measurements were made for scattering angles less than 20^o and energies ranging from 150 eV to 800 eV. Meaningful comparison of the data was possible by using a reduced plot outlined by Smith, Marchi, Aberth, Lorents, and Heinz [10]. This reduced plot consists of plotting $\tau = E\theta$ versus $\rho = \theta \sin\theta\, \sigma(\theta)$. By the use of this scaling law, cross section curves obtained at various energies are reduced to a single line. The reason is that the product $E\theta$ represents essentially the same encounter with the atomic potential. By comparing the data in this manner it was found that the two experimental curves agreed to within a few percent and the unaveraged data infact overlapped. Thus, it was concluded that the experimentally determined cross sections were probably correct. It is further noted that the data of Magnuson, et.al. covered a much larger range of $\tau = E\theta$ than this experiment and does reflect atomic structure such as discussed in the preceeding two paragraphs.

C. MEASUREMENT OF THE $\underline{H}_2^+ + Ar \rightarrow \underline{H}_2^+ + Ar$ CROSS SECTION.

The differential scattering cross section for this reaction was measured from 38.8° to 49.7°. Five runs were made and the data points are displayed in Fig. 19. The average of the 5 runs is displayed in Fig. 20. Important parameters for this measurement included:

(1) Incident energy of H_2^+ ion beam equal to 100 eV.

(2) Focusing magnet current equal to 6.6 amperes.

(3) Solid Angle typically equal to 0.1 steradians.

(4) Argon pressure in the scattering cell typically equal to 1×10^{-3} torr.

From Fig. 20 it is seen that the overall slope of the experimental curve is essentially flat. That the cross section does not decrease significantly with increasing angle is possibly due to the following instrumental effect. Some particles scattered outside of the computed solid angle may reach the detector through multiple collisions with the walls of the apparatus and still have sufficient energy to overcome the detector grid bias. The signal due to these extraneous particles could not be subtracted out in that they essentially behaved like the "real" particles scattered into $d\Omega$. That is, the signal due to extraneous particles was proportional to the incident H_2^+ beam intensity and to the pressure in the scattering cell. Normally, this extraneous signal is negligable compared to the signal from particles scattered within $d\Omega$. However, in this case at the larger angles the

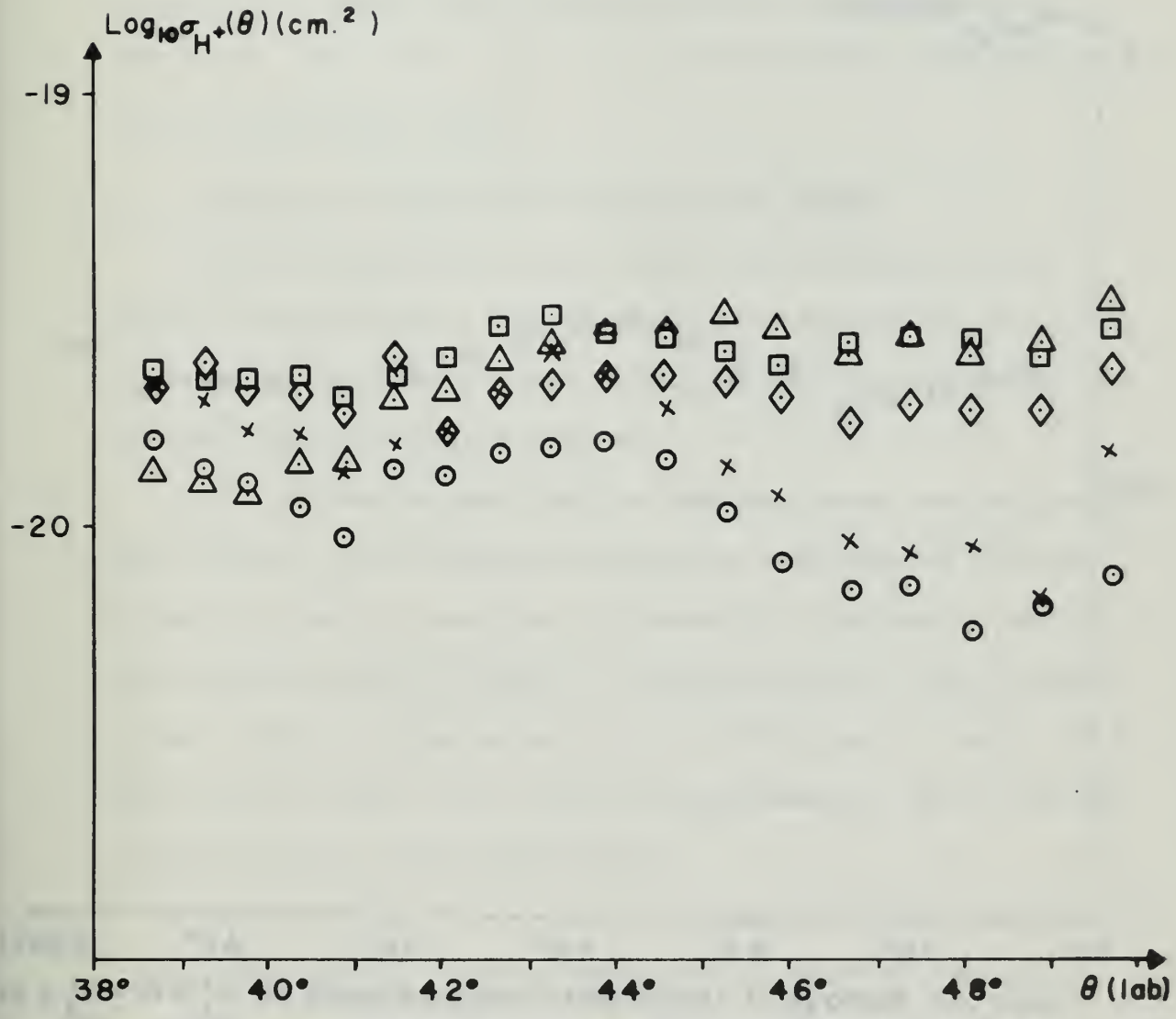

Figure 19. Experimental measurements of $\underline{H_2^+}+Ar \rightarrow \underline{H_2^+}+Ar$ at 100 eV.

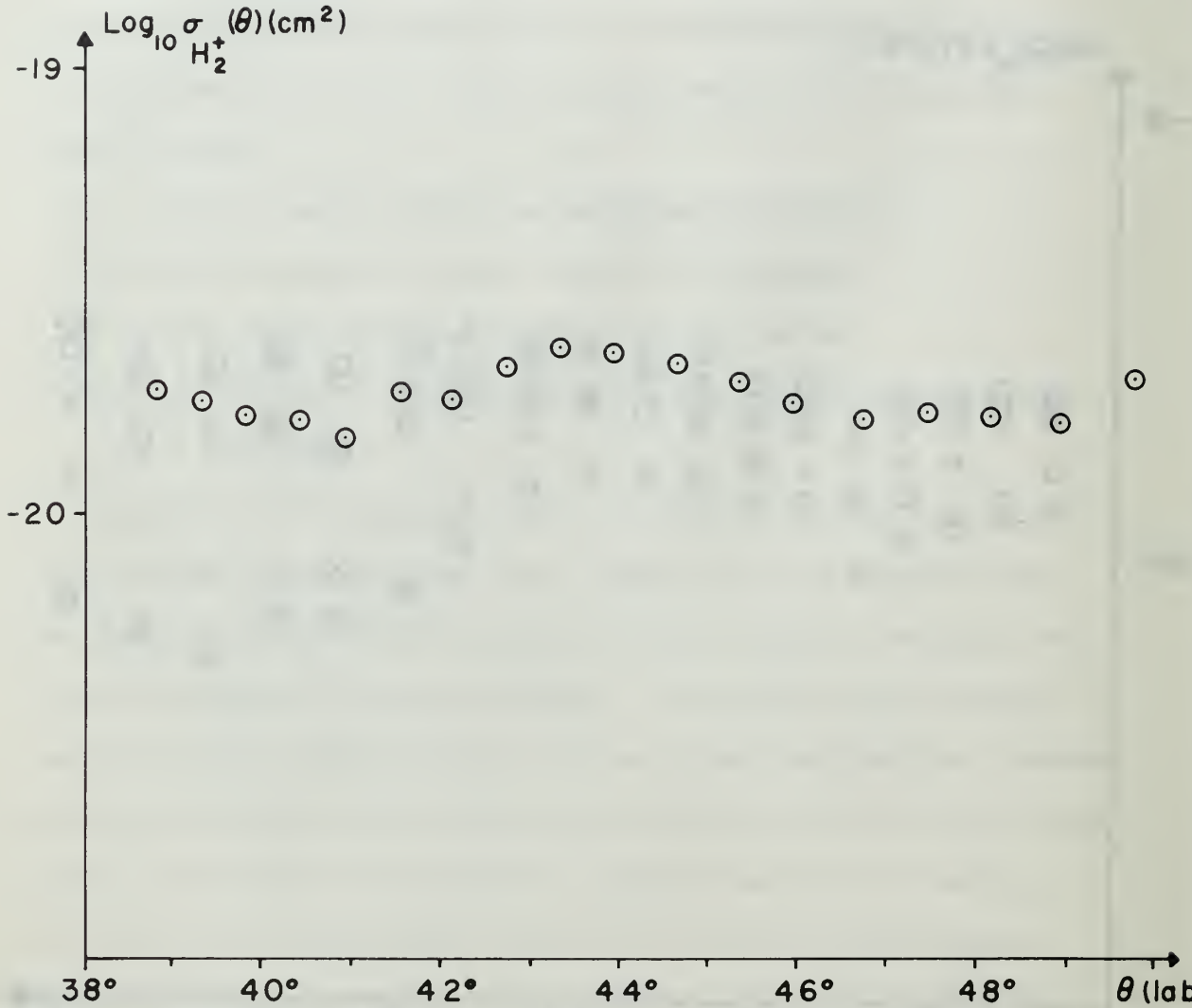

Figure 20. Average of experimental measurements of $\underline{H_2^+} + Ar \rightarrow \underline{H_2^+} + Ar$ at 100 eV.

detector signal was quite small, typically on the order of 0.3×10^{-12} amperes. Therefore, perhaps up to 50 percent of the measured signal could have been due to these extraneous particles. This would also account for the wider dispersion of data at the larger angles.

D. EXPERIMENTAL RESULTS AND THE CLASSICAL MODEL.

Since it could not be assertained with certaintly as to whether the computed or experimental cross section for H^+ on Argon was more accurate, the analysis of the classical model was done from both points of view.

First, it was assumed that the computed cross section for H^+ was correct. The difference between the experimental and computed cross section was then attributed to a systematic error and the experimental H^+ data was normalized to fit the computed curves. This was done by moving the H^+ data up by a factor of 6. Now the H_2^+ on Argon cross section measurement had the following similarities with the H^+ measurement:

(1) Approximately the same focusing magnetic field (see Fig. 16).

(2) Approximately the same excursion in detector position.

(3) Approximately the same calculated solid angle.

(4) The gain curves for both measurements have about the same shape (see Fig. 16).

It was therefore concluded that if a systematic error were present, it should have affected the H_2^+ measurement by about the

same magnitude. Therefore, the H_2^+ data was also increased by a factor of 6. The results of this normalization are shown in Fig. 21. It is seen that the H_2^+ on Argon experimental data presented in this manner lies below the predicted curve by a factor of about 14.

Second, it was assumed that the experimentally measured H^+ on Argon cross section was more accurate than the computed. Since the classical model predicts that the cross section for H_2^+ is proportional to the square of the H^+ cross section (Eq. 8), the predicted curve for H_2^+ on Argon in Fig. 21 would be moved down by a factor of $(6)^2$ or 36. Figure 22 illustrates this. In this case, it is seen that the experimental measurement for H_2^+ on Argon lies below the cross section predicted by the classical model by a factor of about 2 to 3.

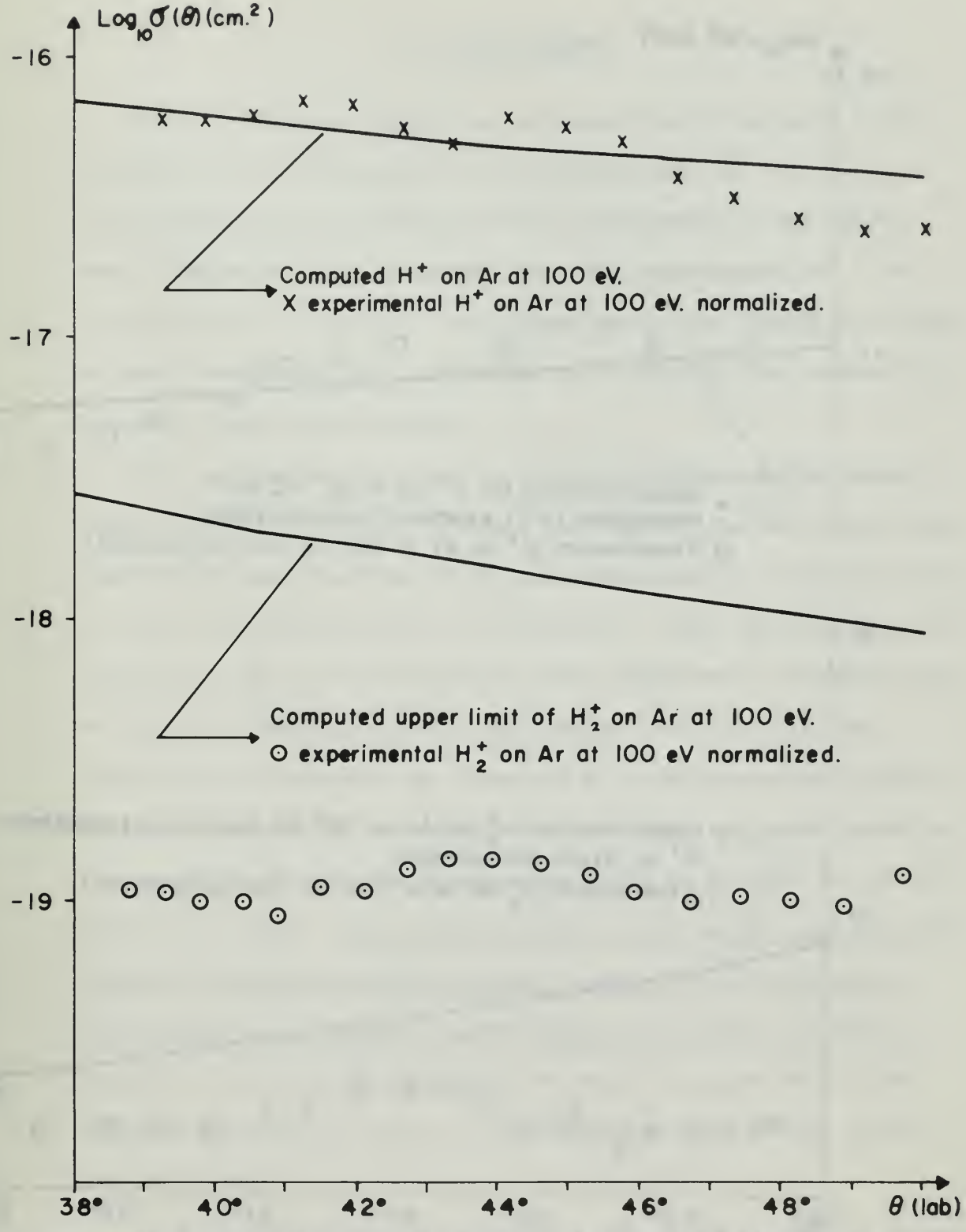

Figure 21. Analysis of experimental measurement assumming a systematic error.

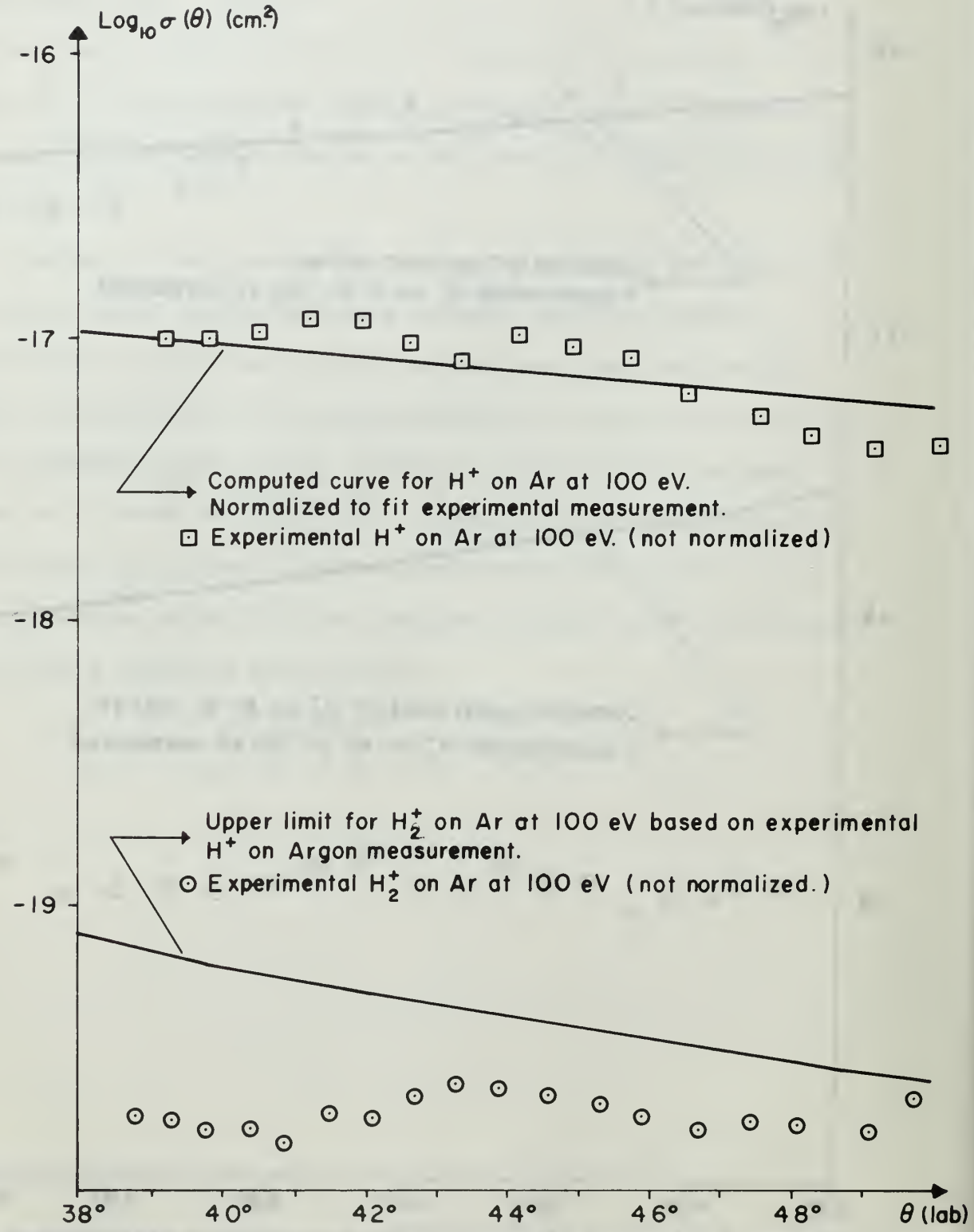

Figure 22. Analysis of experimental measurement assumming no systematic error.

V. CONCLUSIONS

The experimental results given above can be analyzed in two distinct ways: (1) Assume that the theoretical H^+ + Ar curve is correct and that a systematic error was present in the experimental measurements. (2) Assume that the experimental H^+ + Ar cross section is correct. We present below the conclusions based on both assumptions and our reason for believing that method (2) is more likely to be correct.

If a systematic error were present and affected the measurements of both the H^+ and H_2^+ cross sections by the same magnitude, then it was seen that the classical model predicts a cross section for H_2^+ too large by a factor of about 14. That the actual cross section for H_2^+ is so much smaller than predicted is probably due to the two effects previously discussed. That is: (1) the orientation probability was computed by considering the maximum area enclosed by the $\Delta\emptyset = g(\Delta b)$ curve and (2) the model neglected the possibility that the H_2^+ molecule might be excited during the collision process. That the predicted cross section was so much greater than observed would perhaps make the classical model useful only for predicting upper limits of H_2^+ cross sections. However in view of the agreement of our H^+ on Argon data with Magnuson et.al. [9], this is considered the less likely of the two conclusions.

If both experimental measurements are correct, then it is seen that the classical model predicts an H_2^+ cross section too large

by a factor of about 2 to 3. This would make the classical model useful for predicting H_2^+ cross sections on an absolute basis. This is considered to be the more likely of the two conclusions.

Assuming that the classical model is essentially correct the following simple refinement is proposed: Recalling equation (3) it was seen that the orientation probability could be written as

$$P = \frac{S}{2\pi \ell^2}$$

where S was the area enclosed by the $\Delta\emptyset = g(\Delta b)$ curve. Since S could not be determined exactly, an upper limit was obtained by considering the maximum values for $\Delta\emptyset$ and Δb respectively when the other variable was zero. This in fact gave four points on the $\Delta\emptyset = g(\Delta b)$ curve, namely:

$$\Delta\emptyset = 0, \quad \Delta b = + \Delta b_{max}$$

$$\Delta\emptyset = 0, \quad \Delta b = - \Delta b_{max}$$

$$\Delta b = 0, \quad \Delta\emptyset = + \Delta\emptyset_{max}$$

$$\Delta b = 0, \quad \Delta\emptyset = - \Delta\emptyset_{max}$$

A first approximation to the $\Delta\emptyset = g(\Delta b)$ curve can therefore be obtained by simply connecting these points with straight lines. The following sketch illustrates this.

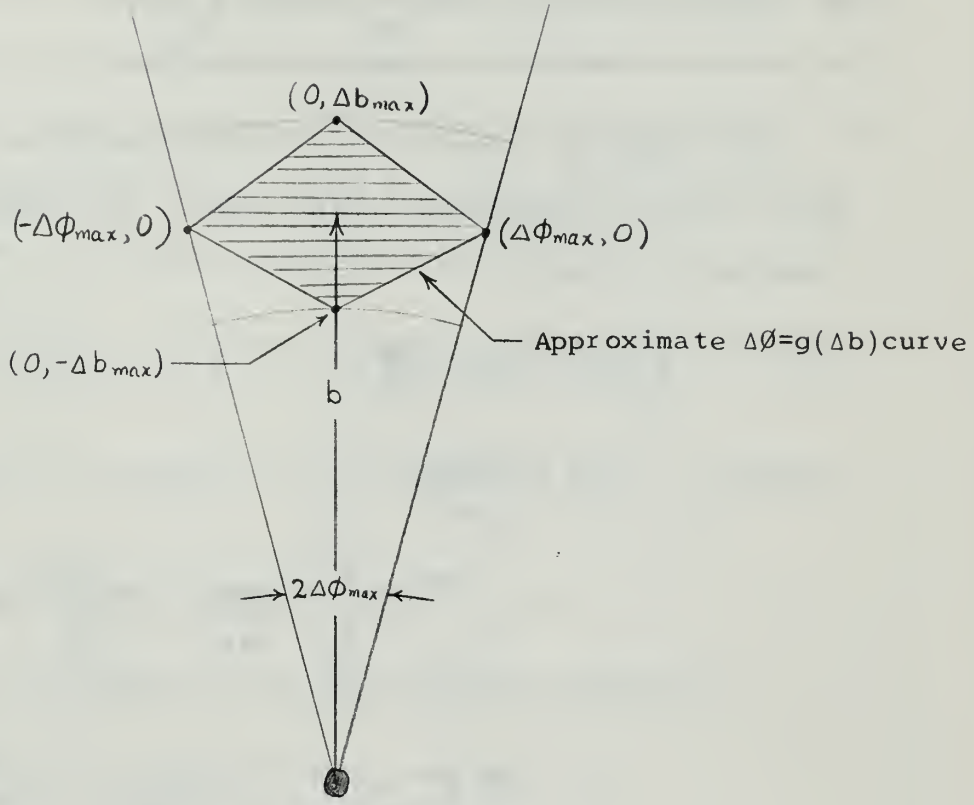

The area enclosed by this first approximation is

$$S = \tfrac{1}{2}[2(\Delta b_{max})\Delta\emptyset = 0][2b(\Delta\emptyset_{max})\Delta b = 0] = \tfrac{1}{2} S_{max}$$

which leads to $P \tilde{=} \tfrac{1}{2} P_{max}$

$$\text{and } \sigma_{H_2^+}(\theta) \tilde{=} \frac{4D}{\pi \ell^2 E_o} [\sigma_{H^+}(\theta)]^2. \qquad (9)$$

Equation (9) predicts the experimentally observed cross section for H_2^+ to within the accuracy of the experiment.

APPENDIX A

1. Computer Program for $\sigma_{H^+}(\Theta)$ and $\sigma_{H_2^+}(\Theta)$.

This computer program solves the following set of equations for classical differential scattering in the center of mass coordinate system.

$$\sigma_{H^+}(\Theta) = \frac{b}{\sin\Theta} \left|\frac{db}{d\Theta}\right|$$

where $\Theta = \pi - 2bU$

$$U = \int_{r_o}^{\infty} \frac{1}{r^2} \left[1 - \frac{V(r)}{\frac{1}{2}\mu V_o^2} - \frac{b^2}{r^2}\right]^{-\frac{1}{2}} dr$$

$$r_o = \text{largest positive root of } 1 - \frac{V(r)}{\frac{1}{2}\mu V_o^2} - \frac{b^2}{r^2} = 0$$

with μ = reduced mass of the system

V_o = velocity of incident particle in the laboratory system

$V(r)$ = scattering potential

In this case the scattering potential as given by Byatt [3] for Argon converted to electron volts is $V(R) = \frac{1}{R}(Ae^{\alpha R} + Be^{\beta R} + Ce^{\gamma R})$ with R in units of Bohr radii (0.5292Å) where

A = 411.4	α = - 1.676
B = -117.5	β = - 3.127
C = 195.9	γ = - 9.625

An outline of this program is as follows:

1. Read in the desired incident energies, mass of proton, mass of target atom, disassociation energy, and potential parameters.

2. Select an impact parameter, b. From an initial value, b is increased in units of .05 a_o where a_o is the first Bohr radius.

3. Solve for the largest positive root of

$$1 - \frac{V(r_o)}{\mu V_o^2/2} - \frac{b^2}{r_o^2} = 0 \text{ using the Newton-Raphson method.}$$

4. Evaluate the integral, $U = \int_{r_o}^{\infty} \left[1 - \frac{V(r)}{\frac{1}{2}\mu V_o^2} - \frac{b^2}{r^2}\right]^{-\frac{1}{2}} \frac{1}{r^2}\, dr$

using the Gauss-Mahler quadrature formula

$$U = \frac{\pi}{r_o}\left[(\cos\tfrac{5\pi}{12})g(x_1)+(\cos\tfrac{3\pi}{12})g(x_2)+(\cos\tfrac{\pi}{12})g(x_3)\right]$$

where $g(x_i) = \left[1 - \frac{V(r_o/x_i)}{\frac{1}{2}\mu V_o^2} - \frac{b^2}{(r_o/x_i)^2}\right]^{-\frac{1}{2}}$

with $x_1 = \cos\frac{\pi}{12}$, $x_2 = \cos\frac{3\pi}{12}$, $x_3 = \frac{5\pi}{12}$. This procedure was taken from Bates, Cook, and Smith [2].

5. From $\Theta = \pi - 2bU$, evaluate $\left|\frac{d\Theta}{db}\right| = \left|2b + 2b\frac{dU}{db}\right|$. $\frac{dU}{db}$ is obtained from the analytic expressions

$U = f(r_o, b)$ and $1 - \frac{V(r_o)}{\mu/2\, V_o^2} - \frac{b^2}{r_o^2} = 0$ in a straight-forward manner using the chain-rule of differentiating $\frac{dU}{db} = \frac{\partial U}{db} + \frac{\partial U}{\partial r_o}\frac{dr_o}{db}$.

6. Solve for $\sigma_{H^+}(\Theta) = \frac{b}{\sin\Theta}\left|\frac{db}{d\Theta}\right|$.

7. Solve for the orientation probability, $P = \frac{8D}{\pi \ell^2 E_o} \sigma_{H^+}(\theta)$.

8. Solve for $\sigma_{H_2^+}(\theta) = P\, \sigma_{H^+}(\theta)$.

9. Write out incident energy, b, r_o, θ, $\sigma_{H^+}(\theta)$, P, $\sigma_{H_2^+}(\theta)$.

Computations are done in units of Bohr radii, but $\sigma_{H_2^+}(\theta)$ and $\sigma_{H_2^+}(\theta)$ are converted to cm^2 at the end of the program. The following is a list of key symbols used in the computer program:

DENER = Disassociation Energy, D, in units of eV.

RHO(J) = Impact parameter, b, in units of Bohr radii.

EV(K) = Incident ion energy in units of eV.

$ET = \frac{1}{2}\mu_{M_{H^+}} EV(K)$ definition

$V = \frac{V(R)\ R}{ET}$ convenient form of the potential in this program

$DV = \frac{dV}{dR}$

DEG(J) = scattering angle in degrees converted to laboratory system

$SIGMA = \sigma_{H^+}(\theta)$

$CS = \sigma_{H_2^+}(\theta)$

```
//    EXEC    FORTCLG,REGION.GO=160K,TIME.GO=10
//FORT.SYSIN    DD  *
C       THIS PROGRAM SOLVES THE CLASSICAL EQUATIONS FOR DIFFERENTIAL
C       SCATTERING
        IMPLICIT REAL*4(A-H,O-Z)
        DIMENSION EV(10),RHO(101),THETA(101),CSL(101),DEG(101),THETAL(101)
        DIMENSION RATIO(10)
C       READ IN POTENTIAL PARAMETERS,BOHR RADIUS,DISSOCIATION ENERGY,
C       INITIAL VALUES
        AO=5.29167E-11
        A=18.0*1.6021E-19*8.9874E+09*(+.84)/AO
        B=18.0*1.6021E-19*8.9874E+09*(-.24)/AO
        C=18.0*1.6021E-19*8.9874E+09*(+.40)/AO
        ALPHA=1.13*2.620741*(-0.566)
        BETA=1.13*2.620741*(-1.056)
        GAM=1.13*2.620741*(-3.25)
        DENER=2.648
        ITN=0
        RHO(0)=-0.05
        EV(0)=600.0
        NO=1
        DO 15 K=1,5
C       THIS DO-LOOP SOLVES PROBLEM AT DESIRED INCIDENT ENERGIES.
        L=K-1
        EV(K)=EV(L)-100.
        R=200./EV(K)
        NO=NO+1
        IF(NO-2)19,16,17
   16   NOA=1
        GO TO 19
   17   NOA=2
        IF(NO-11)19,18,19
   18   NOA=3
   19   CONTINUE
        DO 6 J=1,101
C       THIS DO-LOOP SOLVES PROBLEM AT DESIRED IMPACT PARAMETERS.
        N=J-1
C       THE NEXT 20 STEPS SOLVE FOR 'R',THE DISTANCE OF CLOSEST APPROACH.
        RHO(J)=RHO(N)+0.05
    1   X=EXP(ALPHA*R)
        Y=EXP(BETA*R)
        Z=EXP(GAM*R)
        XMP=1.008
        XMT=39.948
        ET=(0.5*(XMP*XMT)/(XMP+XMT))*EV(K)/XMP
        V=(A*X+B*Y+C*Z)/ET
        G=R**2-V*R-RHO(J)**2
        DV=(A*ALPHA*X+B*BETA*Y+C*GAM*Z)/ET
```

```
      H=V-R*DV+2.*RHO(J)**2./R
      RNEW=R-G/H
      D1FR=ABS((R-RNEW)/RNEW)
      IF(D1FR-0.0001)4,2,2
    2 ITN=ITN+1
      IF(ITN-10000)3,7,7
    3 R=RNEW
      GO TO 1
    4 CONTINUE
      R=RNEW
      V=(A*X+B*Y+C*Z)/ET
      DV=(A*ALPHA*X+B*BETA*Y+C*GAM*Z)/ET
      IF(R-RHO(J))7,120,61
C     THE NEXT 19 STEPS SOLVE FOR 'U',THE INTEGRAL USING A GAUSS
C     QUADRATURE FORMULA
   61 QI=COS(3.14159/12.)
      SJ=COS(3.14159/4.)
      TK=COS((3.14159*5.)/12.)
      QIA=EXP(ALPHA*R/QI)
      QIB=EXP(BETA*R/QI)
      QIC=EXP(GAM*R/QI)
      VI=(A*QIA+B*QIB+C*QIC)/ET
      GI=R/SQRT(R**2.-VI*R*QI-RHO(J)**2.*QI**2.)
      SJA=EXP(ALPHA*R/SJ)
      SJB=EXP(BETA*R/SJ)
      SJC=EXP(GAM*R/SJ)
      VJ=(A*SJA+B*SJB+C*SJC)/ET
      GJ=R/SQRT(R**2.-VJ*R*SJ-RHO(J)**2.*SJ**2.)
      TKA=EXP(ALPHA*R/TK)
      TKB=EXP(BETA*R/TK)
      TKC=EXP(GAM*R/TK)
      VK=(A*TKA+B*TKB+C*TKC)/ET
      GK=R/SQRT(R**2.-VK*R*TK-RHO(J)**2.*TK**2.)
      U=(TK*GI+SJ*GJ+QI*GK)*3.14159/(6.*R)
C     THETA(J),THE SCATTERING ANGLE IN THE CM. IS NOW COMPUTED.
      THETA(J)=3.14159-2.*RHO(J)*U
C     THE NEXT 14 STEPS SOLVE FOR DTHETA.
      DGI=R*RHO(J)*QI**2./(SQRT(R**2.-VI*R*QI-RHO(J)**2.*QI**2.))**3
      DGJ=R*RHO(J)*SJ**2./(SQRT(R**2.-VJ*R*SJ-RHO(J)**2.*SJ**2.))**3.
      DGK=R*RHO(J)*TK**2./(SQRT(R**2.-VK*R*TK-RHO(J)**2.*TK**2.))**3
      DU=3.14159*(TK*DGI+SJ*DGJ+QI*DGK)/(6.*R)
      DRDRHO=2.*RHO(J)/(2.*RHO(J)**2./R-R*DV+V)
      DVI=(A*ALPHA*QIA+B*BETA*QIB+C*GAM*QIC)/ET
      DVJ=(A*ALPHA*SJA+B*BETA*SJB+C*GAM*SJC)/ET
      DVK=(A*ALPHA*TKA+B*BETA*TKB+C*GAM*TKC)/ET
      DGDRI=(DVI/R-QI*VI/R**2.-2.*QI**2.*RHO(J)**2./R**3.)*(GI**3./2.)
      DGDRJ=(DVJ/R-SJ*VJ/R**2.-2.*SJ**2.*RHO(J)**2./R**3.)*(GJ**3./2.)
      DGDRK=(DVK/R-TK*VK/R**2.-2.*TK**2.*RHO(J)**2./R**3.)*(GK**3./2.)
```

```
      DUDR=(TK*DGDRI+SJ*DGDRJ+QI*DGDRK)*3.14159/(6.*R)-U/R
      DUDRHO=DUDR*DRDRHO+DU
      DTHETA=2.*U+2.*RHO(J)*DUDRHO
C     THE CROSS SECTION FOR H+ IS COMPUTED.
      SIGMA=RHO(J)/(SIN(THETA(J))*DTHETA)
C     THETA IS CONVERTED TO LAB COORDINATES.
      ARG=SIN(THETA(J))/((XMP/XMT)+COS(THETA(J)))
      IF(ARG)41,41,42
   41 ARG=1000000
   42 THETAL(J)=ATAN(ARG)
  204 DEG(J)=THETAL(J)*180./3.14159
C     'RAD' IS THE EQUILIBRIUM SEPERATION IN UNITS OF BOHR RADII.
      RAD=1.06/.529167
C     THE ORIENTATION PROBABILITY IS COMPUTED
      P=8.*DENER*SIGMA/(3.14159*RAD*RAD*EV(K))
      IF(P-1.)9,9,8
    8 P=1.
C     'CS' IS THE CROSS-SECTION OF H2+ CONVERTED TO CM.**2.
    9 CS=SIGMA*P*(A0**2.)*10000.
      SIGMA=SIGMA*(A0**2.)*10000.
      IF(DEG(J)-90.)13,6,6
   13 IF(DEG(J)-2.)6,6,12
   12 WRITE(6,5)EV(K),RHO(J),R,DEG(J),SIGMA,P,CS
    5 FORMAT(F8.2,2F12.3,F9.2,1P3E13.3)
    6 CONTINUE
  120 CONTINUE
   15 CONTINUE
    7 CONTINUE
      RETURN
      END
//GO.SYSIN DD *
```

2. Calculation of Ion Trajectory and Solid Angle.

As discussed in Section III E, the scattered ion trajectories and solid angles must be computed numerically. Since much of the computer program that accomplished this is peculiar to the Naval Postgraduate School IBM 360-67 computer installation, only an outline of the program is presented here.

Recall that the axial component of the magnetic field on the magnetic field axis was measured and expressed as a polynomial of the form

$$B_z(z,r = 0) = I \sum_{1}^{13} C_n z^{n-1}.$$

Bush [4] shows that a vector potential for this axially symmetric, non-uniform magnetic field can be written using this expression for $B_z(z,r = 0)$ as:

$$A_\phi(r,z) = \sum_{n=0}^{\infty} \frac{(-1)^n}{n!(n+1)!} \left(\frac{r}{2}\right)^{2n+1} \frac{\partial^{2n} B_z(z,r = 0)}{\partial z^{2n}}$$

$$A_r(r,z) = 0$$

$$A_z(r,z) = 0$$

Using this vector potential in the Lorentz force equation

$$\vec{F} = q\,\vec{v} \times \vec{B} = q\,\vec{v} \times (\vec{\nabla} \times \vec{A}),$$

it follows that:

$$F_r = m\left[\frac{d^2r}{dt^2} - r\left(\frac{d\phi}{dt}\right)^2\right] = q\left[\frac{d\phi}{dt}\frac{\partial(r\,A_\phi)}{\partial r}\right] \qquad (1)$$

$$F_\phi = m\left[2\left(\frac{dr}{dt}\right)\left(\frac{d\phi}{dt}\right) + r\,\frac{d^2\phi}{dt^2}\right] = -q\left[\left(\frac{dz}{dt}\right)\left(\frac{\partial A_\phi}{dz}\right) + \frac{1}{r}\frac{dr}{dz}\frac{\partial(r\,A_\phi)}{dr}\right] \qquad (2)$$

$$F_z = m\left[\frac{d^2z}{dt^2}\right] = q\left[r\,\frac{d\phi}{dt}\frac{\partial A_\phi}{\partial z}\right] \qquad (3)$$

Equation (2) can be reduced to $\frac{d\phi}{dt} = - q \frac{A_\phi}{mr}$. Using this, equations (1) and (3) can be combined to eliminate the time dependence to

$$\frac{\frac{d^2r}{dz^2}}{\left[1+ \left(\frac{dr}{dz}\right)^2\right]} \left[\frac{P^2}{q^2} - A_\phi^2\right] - \frac{dr}{dz}\left[A_\phi \frac{\partial A_\phi}{\partial z}\right] + A_\phi \frac{\partial A_\phi}{\partial r} = 0. \qquad (4)$$

This is a second-order, non-linear differential equation whose solution describes the trajectory of the scattered ion in the magnetic field. In order to integrate it numerically, it is expressed as two first-order, simultaneous differential equations as follows.

Let $y_1 = r$

$$y_2 = \frac{dr}{dz} = \frac{dy_1}{dz}$$

$$f_1 = \frac{A_\phi \frac{\partial A_\phi}{dz}}{\frac{P^2}{q^2} - A_\phi^2}$$

$$f_2 = \frac{A_\phi \frac{\partial A_\phi}{\partial r}}{\frac{P^2}{q^2} - A_\phi^2}$$

Then equation (4) may be equivalently written as

$$\frac{dy_1}{dz} = y_2 \qquad (5)$$

$$\frac{dy_2}{dz} = f_1 y_2^3 - f_2 y_2^2 + f_1 y_2 - f_2 \qquad (6)$$

Equations (5) and (6) were integrated by the DHPGC subroutine which employs a Hamming's modified predictor-corrector method. The solution to (5) and (6) yields the trajectory and hence Z_o and θ_o. Now in a single computer run, the trajectory equations were solved a number of times for various scattering angles. Typically this would be for θ from 35^o to 55^o in 1^o increments. A second subroutine was then called on to generate a seventh order least squares polynomial fit of $\theta = f(Z_o)$. From θ_o and the detector geometry, ΔZ_o was computed. The solid angle could then be computed by the expression

$$d\Omega \cong 2\pi\left(\frac{290}{360}\right) \sin\theta \left|\frac{\partial\theta}{\partial Z_o}\right| \Delta Z_o .$$

The computer output then tabulated θ, Z_o, ΔZ_o, θ_o, and $d\Omega$ as well as a plot of the trajectory (see Fig. 12) if desired.

LIST OF REFERENCES

1. Feist, P.E. Classical Calculation of the Differential Cross Section for Scattering of Hydrogen Molecular Ions From Heavy Atoms, Master's Thesis, Naval Postgraduate School, Monterey, California, June 1967.

2. Bates, D.R., Cook, C.J., and Smith, F.J., "Classical Theory of Ion-Molecule Rearrangement Collisions at High Impact Energies," Proceedings of the Physical Society, V. 83, p. 49-57, (1964).

3. Byatt, W.J., "Analytical Representation of Hartree Potentials and Electron Scattering," The Physical Review, V. 104, p. 1298-1300, 1 December (1956).

4. Bush, T.O. Large Angle Scattering of Lithium Ions by Helium Atoms, Ph.D. Thesis, Naval Postgraduate School, Monterey, California, September 1968.

5. Carter, T.L., Ion Sources for the Production of Low Energy Beams, Master's Thesis, Naval Postgraduate School, Monterey, California, June 1968.

6. Strohsahl, G.H.,Jr., Construction and Calibration of a Mass Spectrometer for the Analysis of Light Ions, Master's Thesis, Naval Postgraduate School, Monterey, California, December, 1967.

7. Kelly, P.J., Analogue Measurements of Charged Particle Trajectories in an Inhomogeneous Magnetic Field, Master's Thesis, Naval Postgraduate School, Monterey, California, 1965.

8. Bush, T.O., Cook, C.J., Heinz, O., and Rodeback, G.W., "Measurement of Large Angle Atomic Scattering Using Axially Symmetric Magnetic Fields," Paper submitted for publication, 1969.

9. Boring, J.W., Magnuson, G.D., and Snyder, R.S., "Elastic Differential Scattering of H^+, He^+, and Ne^{++} by Ar," paper presented at meeting of the American Physical Society, February 1969, St. Louis, Mo. Also private communication in August 1969.

10. Smith, F.T., Marchi, R.P., Aberth, W., Lorents, D.C., and Heinz, O., "Collision Spectroscopy.I. Analysis of the Scattering of He^+ by Ne and Ar,"The Physical Review, V. 161, p. 31-46, 5 September (1967).

11. Aberth, W., and Lorents, C.L., "Elastic Differential Scattering of He^+ Ions by Neon and Ar and of Ar^+ by Ar in the 10-600 eV. Range," The Physical Review, V. 144, p. 109-115, 8 April (1966).

INITIAL DISTRIBUTION LIST

		No. Copies
1.	Defense Documentation Center Cameron Station Alexandria, Virginia 22314	20
2.	Library, Code 0212 Naval Postgraduate School Monterey, California 93940	2
3.	Professor O. Heinz Chairman, Department of Physics Naval Postgraduate School Monterey, California 93940	5
4.	Asst. Prof. R.L. Armstead Department of Physics Naval Postgraduate School Monterey, California 93940	1
5.	LT E.V. Snotherly, Jr., Strategic Systems Projects Office Washington, D.C. 20360	1
6.	Mr. Thomas Maris Department of Physics Naval Postgraduate School Monterey, California 93940	1
7.	LCDR T.O. Bush L-79 Lawrence Radiation Laboratory Box 808 Livermore, California 94550	1
8.	Commander, Naval Ordnance Systems Command Department of the Navy Washington, D.C. 20360	1

Unclassified

Security Classification

DOCUMENT CONTROL DATA - R & D

(Security classification of title, body of abstract and indexing annotation must be entered when the overall report is classified)

1. ORIGINATING ACTIVITY *(Corporate author)*

Naval Postgraduate School
Monterey, California 93940

2a. REPORT SECURITY CLASSIFICATION

Unclassified

2b. GROUP

3 REPORT TITLE

Large Angle Scattering of H^+ and H_2^+ by Argon

4. DESCRIPTIVE NOTES *(Type of report and inclusive dates)*

Master's Thesis; October 1969

5. AUTHOR(S) *(First name, middle initial, last name)*

Everrette V. Snotherly, Jr.

6. REPORT DATE	7a. TOTAL NO. OF PAGES	7b. NO. OF REFS
October 1969	72	11

8a. CONTRACT OR GRANT NO.	9a. ORIGINATOR'S REPORT NUMBER(S)
b. PROJECT NO.	
c.	9b. OTHER REPORT NO(S) *(Any other numbers that may be assigned this report)*
d.	

10. DISTRIBUTION STATEMENT

This document has been approved for public release and sale; its distribution is unlimited.

11. SUPPLEMENTARY NOTES	12. SPONSORING MILITARY ACTIVITY
	Naval Postgraduate School Monterey, California 93940

13. ABSTRACT

The elastic differential scattering cross sections for $\underline{H}^+, \underline{H}_2^+ + Ar \rightarrow \underline{H}^+, \underline{H}_2^+ + Ar$ were measured for angles of 39^o to 50^o with incident lab energy of 100 eV. The apparatus utilized the properties of axially symmetric, non-uniform magnetic fields (large thin solenoid) to focus all scattered ions with vector momentum $\vec{p}$ within $\Delta\vec{p}$ onto a detector placed down the magnetic axis. Thus, the solid angle was increased by a factor of about 300 over conventional methods with comparable resolution in $\Delta\theta$ (about 1^o). A typical value for $\sigma_{H^+}(43^o)$ is $8.2 \times 10^{-18} cm^2$. The H^+ data was compared with data of Magnuson, et.al., via a scaling law and was in excellent agreement. A typical value for $\sigma_{H_2^+}(43^o)$ is $2.4 \times 10^{-20} cm^2$. A simple refinement of a classical model for H_2^+ scattering by Feist relates these cross sections by $\sigma_{H_2^+}(\theta) = P\,\sigma_{H^+}(\theta) \simeq \frac{4D}{\pi \ell^2 E_o} [\sigma_{H^+}(\theta)]^2$ where P is an orientation factor, D the binding energy, and ℓ the internuclear separation. This expression relates the cross sections to within the accuracy of the experiment thus verifying the classical approximations.

DD FORM 1 NOV 65 1473 (PAGE 1)

S/N 0101-807-6811

Unclassified

Security Classification

A-31408

14. KEY WORDS	LINK A		LINK B		LINK C	
	ROLE	WT	ROLE	WT	ROLE	WT
Differential scattering of H^+ by Argon						
Differential scattering of H_2^+ by Argon						
Large angle scattering cross section						
Axially symmetric magnetic field focusing						
Orientation probability						
Classical Impulse Approximation						